RESEARCH

Association of Mesoscale Features With Tropical Cyclone Tauktae

Nandivada Umakanth[1] · Prathipati Vinay Kumar[2] · Rupraj Biswasharma[1] · Rajesh Gogineni[3] ·
Shaik Hasane Ahammad[4] · Myla Chimpiri Rao[5]

Abstract

An attempt has been made in this paper to examine the ability of various microphysical schemes (Morrison, Thompson, Lin) of Weather Research Forecasting (WRF) model in analyzing the convective features in a cyclone Tauktae over the Arabian Sea from May 14th to May 19th, 2021. This study explores the model's performance of various schemes with MERRA2 observations. For rainfall, India Meteorological Department (IMD) daily rainfall dataset has been considered as observation. In this study, the evaluation of various model parameters has been done using statistical metrics and skill scores. Among the three schemes, Morrison scheme stands out to be most reliable scheme with high correlation and less BIAS and Root Mean Square error (RMSE). The convective parameters used for the study of cyclonic activity are rainfall (RF), cloud top temperature (CTT), lifted index (LI), total precipitable water (TPW), convective available potential energy (CAPE), convective inhibition (CIN), sea level pressure (SLP), sea surface temperature (SST), geo potential height (GPH), Storm Relative Helicity (SRLH), composite reflectivity (COMP_ref) and divergence. CAPE has been a useful parameter in analyzing the cyclone's energy. The WRF model was found to be useful in forecasting severe convection related cyclonic activity.

Keywords Cloud top temperature · Sea level pressure · Sea surface temperature · Convective inhibition

Introduction

North Indian Ocean (NIOC) is known to be one of the warmest oceanic waters that favours the production of tropical cyclones. The NIOC accounts for 7% of total cyclonic events across all oceans. NIOC comprises of two gigantic seas. One is Bay of Bengal Sea (BOBS) and other one is Arabian Sea (ARBS). When compared to the other oceanic water, the cyclones originated in NIOC cause severe destruction during landfall. In the last 100 years, nearly 75% of extreme disastrous cyclones took place in NIOC basin (Manche et al. 2024; Mohanty et al. 2012; Johnson and Xie 2010; Walsh et al. 2016; Raju et al. 2022; Swapna et al. 2023). During 1970-2004, the occurrence of severe cyclones across all oceans took place in tropics. Increased SST and High intensity winds (>60 m/s) are feeding the intense cyclonic activities in the tropics (Webster et al. 2005; Hoyos et al. 2006; Pirro et al. 2020). During 1970-2000, severe cyclones with wind speeds greater than 50 m/s are becoming more often in NIOC seas. As per the Indian Meteorological Department (IMD) cyclone atlas, the occurrence of severe cyclones with wind speeds more than 25 m/s had grown by 41% in NIOC seas (Singh et al. 2000; Mohanty et al. 2012).

Fragile vertical wind shear, low level vorticity, high relative humidity, SST >26° C and conditional instability are the major weather conditions that favour for the development of cyclonic activity (Gray 1968). Even when conditions are good over tropical waters at any given time, only a small portion of dense cloud groups go on to form tropical storms. The study by Gray (1968) identified a presence of vertical shear in easterly winds that helps for the seasonal shift in the monsoonal trough across India. This helps deep

✉ Myla Chimpiri Rao
  raomc72@gmail.com

1 Indian Institute of Tropical Meteorology (IITM), Dr. Homi Bhabha Road, Pashan, Pune, Maharashtra 411008, India

2 Department of Meteorology and Oceanography, College of Science and Technology, Andhra University, Visakhapatnam 530003, India

3 Department of ECE, Dhanekula Institute of Engineering and Technology, Vijayawada 521139, India

4 Department of ECE, Koneru Lakshmaiah Education Foundation, Vaddeswaram 522502, India

5 Department of Physics, Andhra Loyola College, Vijayawada 520008, India

depressions and cyclones to form in the months of July and August. The study also reveals that cyclones in ARBS occur due to the movement of monsoon trough during pre-monsoon and post-monsoon seasons. In Pre-monson season, the monsoon trough moves northward whereas in post-monsoon season it moves southward. The study also suggested that the poleward moment of trough is being favored by vertical wind shear. Usually the trough moves meridionally between 5° and 10°N. The storms originating in ARBS during pre-monsoon are very severe. The cyclonic circulations across ARBS were strengthened by the strengthening of low-level westerlies that are influenced by outflow of upper level air. In few occasions, hadley cell also played a significant role in the occurrence of tropical cyclones (Maloney et al. 2019). For better understanding of the westerly winds, genesis potential (GP) indicator serves as a useful tool (Camargo et al. 2009; Emmanuel et al. 2021). The GP values are very high during the active phase of Madden–Julian oscillation (MJO) over NIOC. The MJO creates a significant impact on the cyclonic occurrence across the ARBS (Wheeler and Hendon 2004; Singh et al. 2000; Camargo et al. 2010).

In few occasions, latent and sensible heat fluxes act as major source for the potential energy. The differences between these fluxes and sea surface help to develop a convective instability in tropical cyclones. This instability increases due to heating of oceanic waters and moisture supply. For instance, a tropical cyclone may include a group of convective cells and meso scale convective systems at various stages of its development. The convective systems are linked with relative vorticity in lower tropospheric levels (Houze et al. 2009).

Recent studies have given sufficient evidence regarding the fast development of intense convective systems into cyclonic disturbances (Nolan 2007; Dunkerton et al. 2009; Deshpande et al. 2012; Montgomery et al. 2012; Wang et al. 2010).

CAPE is one of the important factors that contribute for the deep convective systems. Few Observational studies indicated that wind shear in a tropical cyclone is linked with the asymmetrical distribution of moisture. This increases instability that contributes for a larger CAPE values in a cyclonic disturbance. CIN triggers the down shear of a wind that increases the convective instability. In the tropical cyclone formation, convective systems and extreme rainfall are highly correlated to the TPW and relative humidity in the atmosphere. The instability indices are the main parameters used to assess the formation of deep moist convection and severe weather. Temperature and humidity profiles in the atmosphere are used to calculate them. Due to the significant advancement in satellites, we can estimate those instability indices from the satellite datasets rather than depending on radiosonde observations (Balaguru et al. 2014; Ali et al. 2013; Wing et al. 2019; Umakanth et al. 2022; Rajesh and

Babu 2012; Sangani et al. 2021; Gogineni and Sangani 2022; Chen et al. 2020; Molinari et al. 2012). Conte et al. (2011) conducted a research to assess a cyclone based on several stability indices. They came to the conclusion that deep convection development is greatly supported by the KI, LI, CAPE, and TPW factors. Additionally, they demonstrated a direct correlation between indices and the cyclone's frontal system. The start of the severe cyclonic downpour is accompanied by a rise in the CAPE value, since it is well known that the cyclone's eye is essentially encircled by huge thunderstorms. They also revealed that low values of LI parameter are a good precursor for high atmospheric instability.

Reanalysis datasets are very helpful for analyzing the climatology of tropical cyclones. They help us to understand the influence of large scale circulations on cyclonic formations. Scoccimarro et al. (2017) revealed that reanalysis dataset can be used as major assessing dataset for analyzing tropical storm inner core dynamics and interactions with the climate system. Schenkel and Hart (2012) also looked into the reanalysis data sets that are commonly utilized in determining the position of tropical cyclones and their life spans throughout multiple ocean basins. Based on the above studies, we have considered the reanalysis datasets as an observation for our study. The structure of the paper is as follows: Section "Observed Features Data and Methodology" of the study's methodology and data are discussed. The results are discussed in detail in Section 3, and the most significant conclusions are outlined in Section "Conclusions".

Observed Features, Data and Methodology

Observed Features Associated with Tauktae

The Indian Meteorological Department (IMD) categorizes Cyclone Tauktae as an Extremely Severe Cyclone on May 14th, 2021. It was the fifth-most potent cyclone seen in the month of May across Arabian sea. The name of the tropical cyclone Tauktae, sometimes known as Tau'Te, comes from Myanmar, which is next to India and symbolizes the gecko, a particularly loud animal there. The Tauktae name for the tropical cyclone was suggested by the Indian Meteorological Department (IMD) (Rathore et al. 2017). On May 13, 2021, a highly potent tropical cyclone known as "Tauktae" was born over the Arabian Sea. On May 13, 2021, a low-pressure system for the six-day devastating cyclone Tauktae first surfaced in the ARBS. The low pressure system moved eastward and developed a severe depression by May 14th. On May 14th, 2021, the cyclone started moving eastward direction. Later, it moved mostly towards north direction as it gets intensified. Warm waters near the beach caused the storm to quickly travel northward. Later that day, the storm was upgraded to a cyclonic storm and given the name

Tauktae. On May 15, Tauktae gained additional strength and later that day developed into a strong cyclonic storm. Early on May 16th, Tauktae started to move parallel the shores of Kerala, Karnataka, Goa, and Maharashtra before quickly intensifying into a very violent cyclonic storm. On May 17, 2021, it made landfall in the Indian state of Gujarat, some 27 kilometres east of Diu. After reaching landfall, the storm moved farther inland before gradually losing strength and dissipating on May 19, 2021, as a low-pressure system. With maximum 3-minute sustained winds of 195 km/h and maximum 1-minute sustained winds of 220 km/h, as well as a minimum central pressure of 950 millibars, Tauktae was at its strongest when it made landfall on the Gujarat coast, making it the equivalent of a Category-4 tropical cyclone on the Saffir-Simpson scale1. The country's southern regions experienced intense rainfall as a result of the cyclone's extensive area of convection. Previous studies on Tauktae event have mainly discussed the atmospheric interactions between land and ocean. In this study, we mainly discussed about the convective features in cyclone Tauktae event as identified by the MERRA2 satellite reanalysis dataset and WRF model.

Data

The link https://disc.gsfc.nasa.gov/datasets?project= MERRA-2 was used to gather Modern Era Retrospective Analysis for Research and Application (MERRA) data with 0.5° resolution for the time range of May 14–19, 2021. Using MERRA2 temperature and relative humidity pressure level data, the CAPE, CIN, TPW, and LI parameters are determined (Gelaro et al. 2017). India Meteorological Department (IMD) gridded daily rainfall data (https://www.imdpune.gov. in/cmpg/Griddata/Rainfall_25_NetCDF.html) for the Indian subcontinent at 0.25 degree resolution for the time period May 14–19, 2021 has been collected (Pai et al. 2014).

Methodology

For our study, we calculate few parameters using the formulas mentioned below.

(i) Convective available potential energy (CAPE)
    The formula by Moncrieff and Miller (1976) is utilised to calculate CAPE.

$$CAPE = \int_x^y g[\frac{TV_{parcel} - TV_{env}}{TV_{env}}]dz \qquad (1)$$

where TV_{parcel} represents the virtual temperature of the parcel and TV_{env} represents the virtual temperature of the surroundings respectively. The variables

x and y stand for the levels of free convection and neutral buoyancy.

(ii) Lifted Index (LI)
    Galway (1956) has developed this index to assess the instability in the lower levels of the troposphere.

$$LI = a_{500} - a_{parcel} \qquad (2)$$

where 'a' denote air temperature and 'a_{parcel}' denote parcel's temperature that is being elevated from the ground to a pressure level of 500 hpa.

(iii) Total precipitable water (TPW)
    TPW is mainly used to estimate the amount of water vapour present in the atmosphere. It can be computed using the formula below:

$$TPW = \frac{1}{g}\int_{P_1}^{P_2} W\,dP \qquad (3)$$

where P_1 and P_2 indicate the levels related to pressure, W denotes mixing ratio(Carlson et al. 1990)

(iv) Convective Inhibition (CIN):
    Parker (2002) has utilised the CIN formula to measure the amount of energy required for the lifting of the air parcel in the cyclone development.

$$CIN = \int_{Z_l}^{Z_f} g[\frac{T_{v,parcel} - T_{v,\,env}}{T_{v,env}}]dz \qquad (4)$$

where $T_{v,parcel}$ indicates the virtual temperature of the parcel and $T_{v,env}$ represents the virtual temperature of the surroundings respectively. Z_f demonstrates the level of free convection and Z_l denotes the surface level.

(v) Dew point depression (DPT): It is computed by subtracting the air temperature and the dew point temperature (Umakanth et al. 2020).

(vi) Storm Relative Helicity (SRLH):
    SRLH is calculated using the formula (Rasmussen and Blanchard 1998).

$$SRLH = \int_0^h \vec{k}.(\vec{V} - \vec{C})X\frac{d\vec{V}}{dz}dz \qquad (5)$$

where V is the wind vector in the environment, C is the storm's translation velocity, k x dV/dz is the horizontal vorticity and k is the vertical unit vector. SRLH is mainly linked with deeper layer vertical wind shear that plays crucial role in super cell development. In general, higher SRLH values indicate the evolution of super cells that pose a greater threat for the occurrence of tornadoes.

To assess the effectiveness of the MERRA2 and WRF model in the study, statistically based analy-

sis was also conducted. The correlation coefficient (CC), root-mean-square error (RMSE), and BIAS terms were computed using the following formulas (Wilks 2006):

$$BIAS = \frac{1}{n} \sum_{i=1}^{n} (o_i - f_i) \qquad (6)$$

$$CC = \frac{\sum_{i=1}^{n} \left(f_i - f' \right) \left(o_i - o' \right)}{\sqrt{\sum_{i=1}^{n} \left(f_i - f' \right)^2} \sqrt{\sum_{i=1}^{n} \left(o_i - o' \right)^2}} \qquad (7)$$

$$RMSE = \sqrt{\frac{\sum_{i=1}^{n} (f_i - o_i)^2}{n}} \qquad (8)$$

where o_i and f_i indicate the values of observation and predicted; f' represents the mean of all the predicted values; o' represents the mean of all the observed values.

Skill Score for WRF

Skill score has been used as one of the effective way to assess the forecast skill. This assessment is based on the contingency table (Table 1) (Mukhopadhyay et al. 2003; Haklander and Delden 2003; Tyagi et al. 2011). In order to understand the performance of the CAPE, CIN and LI to detect convection, the following multiple skill scores are calculated from contingency table (Table 1) based on the observed and simulated results (i) Probability of Detection (POD), (ii) False Alarm Ratio (FAR), (iii) Critical Success Index (CSI), (iv) True Skill Statistic (TSS), (v) Miss rate (MR) and (vi) Percent Correct (PC).

$$POD = \frac{A}{A + B} \qquad (9)$$

$$FAR = \frac{C}{A + C} \qquad (10)$$

$$CSI = \frac{A}{A + B + C} \qquad (11)$$

Table 1 Contingency Table used for skill score assessment

	Reported	Forecasted
A	YES	YES
B	YES	NO
C	NO	YES
D	NO	NO

$$TSS = \frac{AD - BC}{(A + B)(C + D)} \qquad (12)$$

$$MR = \frac{B}{A + B} \qquad (13)$$

$$PC = \frac{A + D}{A + B + C + D} * 100 \qquad (14)$$

where Total no. of events $N = A + B + C + D$

Expected no. of correct forecast by chance $E = [(A + C)(A + B) + (C + D)(B + D)]/N$

$CF = A + D$

Weather Research Forecasting Model (WRF)

The National Center for Atmospheric Research (NCAR) developed this model in collaboration with the National Center for Environmental Prediction (NCEP) of the National Oceanic and Atmospheric Administration (NOAA). Using the FNL (Final) Operational Global Analysis data from the NCEP, the model's fundamental initial conditions were gathered with a spatial resolution of 1 degree (https://rda.ucar.edu/datasets/ds083.2/). In order to achieve the goal of cyclone prediction, the WRF model run was simulated for single horizontal domain at a 27 km resolution (Fig. 1). The ARBS region that was selected for the prediction of WRF model in this research lies between 0°N and 30°N latitude and 45°E and 85°E longitude. The WRF model version 3.6.1 was employed (Skamarock et al. 2019). The model uses primitive equations and non-hydrostatic equations for dynamics. The model's ideal number of vertical levels was 42. We used the rapid radiative transfer model (RRTM) scheme for long wave radiation during the model run and the Dudhia method for short wave radiation. The model utilised the traditional, streamlined cumulus convection method of Grell-Freitas ensemble scheme. For the planetary boundary layer, we employed the Yonsei University Scheme. Regarding microphysics schemes, the study investigated three different options, including the Lin et al. Scheme (Lin) (Lin et al. 1983), Thompson Scheme (Thompson) (Thompson et al. 2008), Morrison Scheme (double-Moment) (Morrison et al. 2009, 2015; Biswasharma et al. 2024). The Morrison scheme is a double moment scheme and includes Vapor, cloud water, rain water, cloud ice, rain, snow and graupel. The Thompson scheme includes six prognostic equations of hydrometeors and the number concentrations for ice and rain. The Lin scheme treats mixed-phase processes and predict six hydrometeors: water vapor, cloud water, cloud ice, rain, snow and graupel. The Revised MM5 Monin-Obukhov Scheme was used to study surface layer physics. Table 2 lists the model's most important characteristics. For the land surface, we utilised the Noah Land Surface Model.

Fig. 1 Model domain for numerical experiments
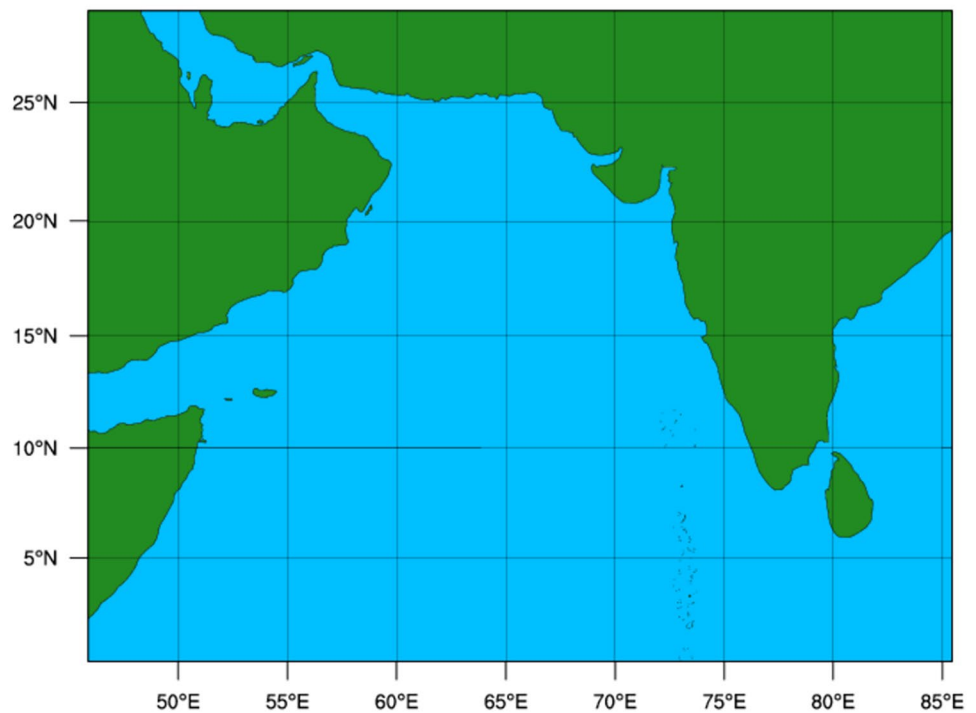
The model run was started from 1200UTC on May 13th, 2021 to 0000UTC on May 20th, 2021. The WRF model is integrated continuously for 156 hrs and the predicted atmospheric variables for the later 144-hr period (first 12-hr output is discarded as of model spin-up).

Results and Discussion

The major aim behind this study is to understand the ability of various schemes of WRF model in analyzing the convective features in a cyclone. In evaluating the model's performance of various schemes, observational data over the study region has been compared with the model- simulated

Table 2 Model Details

Model features	Specifications
Horizontal resolution	27 km
Vertical levels	42 levels
Radiation	RRTM scheme for long wave Dudhia scheme for short wave
Cu_physics	Grell-Freitas ensemble scheme
Planetary boundary layer	Yonsei University Scheme
Mp_physics	Morrison scheme
Surface layer physics	Revised MM5 Monin-Obukhov Scheme
Land surface physics	Noah Land Surface Model

results. For rainfall purpose, we have used IMD daily rainfall as observation. For other parameters, we have utilized, MERRA2 dataset as observational purpose. A total of three different microphysics schemes (Morrison, Thompson and Lin) (Skamarock et al. 2019) were used in the sensitivity experiments for analyzing the cyclone keeping the other physics options unaltered. We have used correlation coefficient, RMSE and BIAS for each microphysics scheme in reference to our observation. We also evaluated skill scores for each microphysical scheme. We observe that Morrison scheme showed good correlation than other two schemes. Out of all parameters, all model simulations showed GPH parameter has highest correlation and COMP_ref showed lowest correlation with observation (Table 3). As rainfall is one of the important factor in the cyclone, Morrison showed less RMSE and BIAS when compared to other models (Tables 4 and 5). For CAPE simulations, Morrison showed high correlation (~0.739) and less RMSE (550.40), BIAS (162.08) when compared to other models (Tables 4 and 5). Lin scheme showed poor correlation (~0.253) with observation. As we are analyzing the convective features in the cyclone, we calculated skill scores for CAPE, CIN and LI. In these three parameters, Morrison showed high POD, CSI & TSS and less FAR, MR with respective to Thompson and Lin (Tables 6, 7 and 8). The tracks of cyclone Tauktae simulated by the three different experiments along with the observed track (IMD best track data) are presented in Fig. 2.

Table 3 Correlation for Different WRF schemes

	Morrison	Thompson	Lin
RF	0.757	0.706	0.506
CAPE	0.739	0.621	0.253
CIN	0.609	0.465	0.240
LI	0.603	0.224	0.136
COMP_ref	0.547	0.217	0.199
SRLH	0.651	0.537	0.269
RH	0.736	0.640	0.347
DPT	0.786	0.608	0.282
GPH	0.840	0.716	0.577

Table 4 RMSE for Different WRF schemes

	Morrison	Thompson	Lin
RF	8.428	12.933	18.076
CAPE	550.407	618.531	826.517
CIN	318.634	397.640	428.409
LI	1.985	2.301	4.143
COMP_ref	17.862	19.287	19.753
SRLH	23.371	37.886	38.097
RH	18.718	24.079	28.690
DPT	69.613	78.836	81.940
GPH	347.544	407.685	477.655

Table 5 BIAS for Different WRF schemes

	Morrison	Thompson	Lin
RF	4.029	9.610	15.247
CAPE	162.086	187.709	247.064
CIN	112.013	162.985	229.821
LI	-0.554	-1.830	-2.473
COMP_ref	7.446	8.206	8.831
SRLH	4.763	6.010	15.408
RH	1.989	5.526	6.473
DPT	59.266	67.517	72.495
GPH	292.365	331.515	388.389

Table 6 Skill score evaluation of WRF Morrison scheme and MERRA2 for CAPE, CIN & LI parameters

Skill	CAPE	CIN	LI
POD	0.77	0.60	0.45
FAR	0.36	0.27	0.44
CSI	0.53	0.49	0.33
TSS	0.36	0.32	-0.07
MR	0.22	0.39	0.54
PC	67.74	65.59	46.23

Table 7 Skill score evaluation of WRF Thompson scheme and MERRA2 for CAPE, CIN & LI parameters

Skill	CAPE	CIN	LI
POD	0.62	0.46	0.34
FAR	0.55	0.60	0.5
CSI	0.35	0.27	0.25
TSS	0.27	0.15	-0.22
MR	0.37	0.53	0.65
PC	64.51	62.36	37.63

Table 8 Skill score evaluation of WRF Lin scheme and MERRA2 for CAPE, CIN & LI parameters

Skill	CAPE	CIN	LI
POD	0.42	0.39	0.21
FAR	0.41	0.40	0.45
CSI	0.32	0.31	0.18
TSS	0.25	0.21	-0.04
MR	0.57	0.60	0.78
PC	68.81	64.51	43.01

In this case, the Morrison scheme produced better track than the other schemes. These results also corroborate with the previous study by Mohan et al. (2019) showing that Morrison scheme has influence of microphysics on track assessment. Among the Microphysics schemes tested, Morrison emerges as the optimal choice within these combinations. Thompson is the second best option in assessing the convective features of a cyclone. Among three schemes, Lin scheme showed poor correlation for convective assessment of cyclone Tauktae. We are presenting the various features of the tropical cyclone Tauktae simulated from the Morrison scheme in this study. Rainfall (RF), cloud top temperature (CTT), lifted index (LI), total precipitable water (TPW), sea level pressure (SLP), convective available potential energy (CAPE), sea surface temperature (SST), convective inhibition (CIN) and divergence are the variables used to analyze the cyclonic activity.

Discussion of RF and CTT with Cyclone Tauktae

Figure 3 shows the simulated rainfall pattern across the Arabian Sea region from May 14th to 19th, 2021. High intensity rainfall was observed near the Kerala and Karnataka coasts on May 14th, 2021. The rainfall values range between 10 and 100 mm over ARBS (Fig. 3(a)). On 15th May, 2021, High intensity rainfall was observed near Karnataka and Maharashtra coastal areas. The rainfall values range between 60 and 100 mm over ARBS (Fig. 3(b)). On 16th May, 2021, High intensity rainfall was observed near Maharashtra coastal areas. The rainfall values range between 60 and 100 mm over ARBS (Fig. 3(c)). On 17th May, 2021, High intensity rainfall was observed near Gujarat coastal areas. The rainfall values range between 40 and 100 mm over ARBS (Fig. 3(d)).

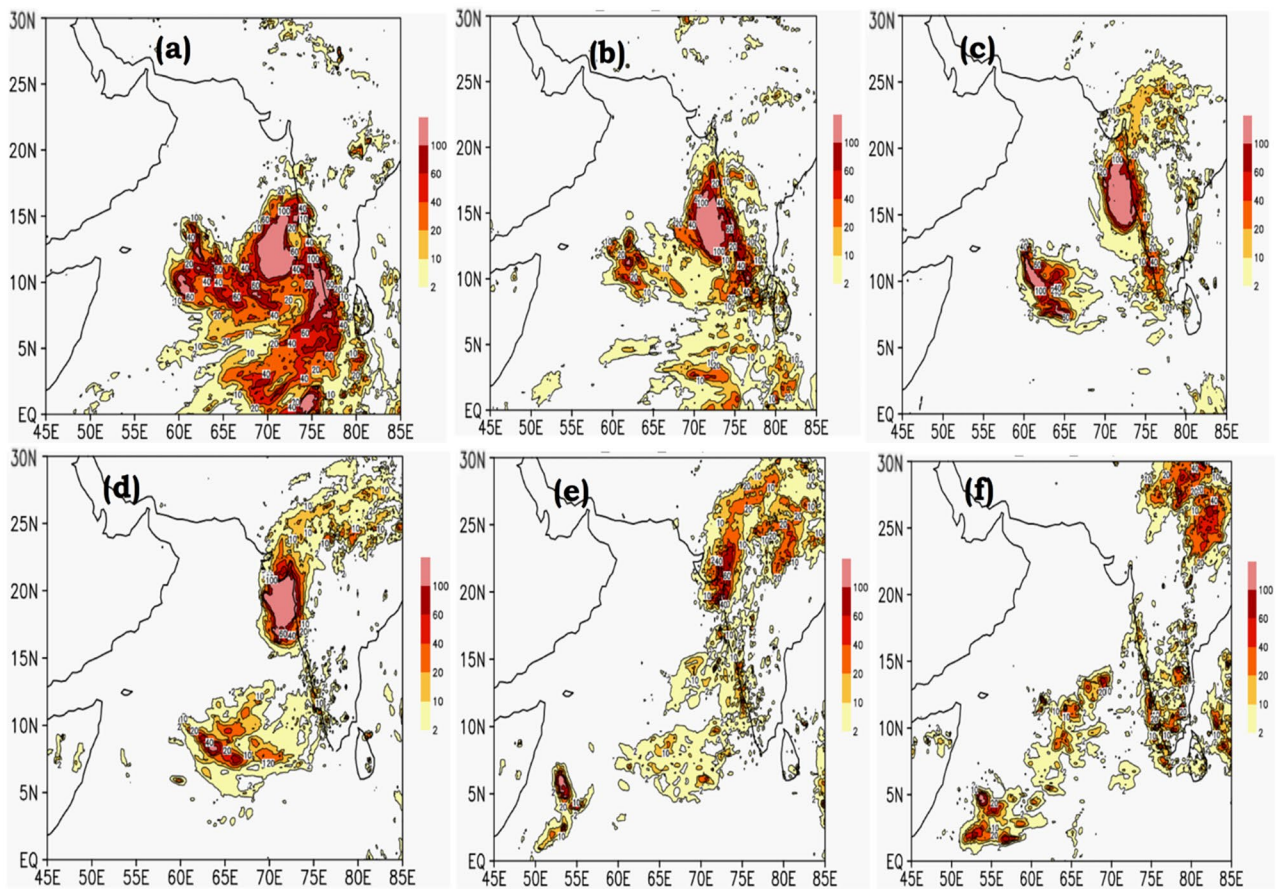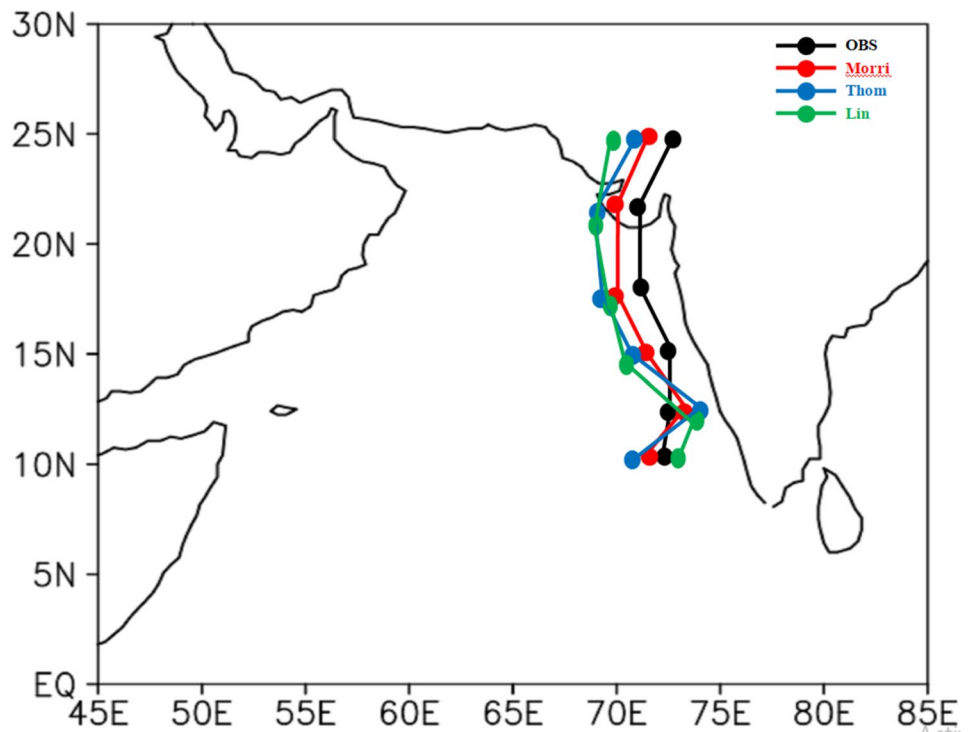**Fig. 2** Simulated tropical cyclone track with observation (IMD)

Fig. 3 Spatial distribution of WRF simulated mean daily rainfall during **a** May 14th, 2021, **b** May 15th, 2021, **c** May 16th, 2021, **d** May 17th, 2021, **e** May 18th, 2021, **f** May 19th, 2021

On 18th May, 2021, the rainfall activity has been decreased near Gujarat. The rainfall values range between 10 and 40 mm over ARBS (Fig. 3(e)). On 19th May, 2021, no rainfall was seen near Gujarat and Maharashtra coastal areas over ARBS (Fig. 3(f)). Figure 4(a-f) shows the IMD rainfall pattern across the Arabian Sea region from May 14th to 19th, 2021. On May 14th, 2021 High intensity rainfall of 60-100 mm was observed near the Kerala coastal region. On May 15th, 2021 High intensity rainfall of 70-100 mm was observed near the Kerala and Karnataka coastal regions. On May 16th, 2021 High intensity rainfall of 80-100 mm was observed near the Maharashtra coastal regions. On 17th & 18th May, 2021 high intensity rainfall was observed near Gujarat coastal areas. The Morrison scheme simulated rainfall patterns were indicating the same intensity of rainfall matching with the IMD rainfall. These results also corroborate with the previous studies by Mohan et al. (2018), Reddy et al. (2022) and Biswasharma et al. (2024) showing that Morrison scheme has been a good choice in assessing the rainfall occurrence.

Figure 5 shows the simulated CTT pattern across the Arabian Sea region from May 14th to 19th, 2021. On 14th May, 2021 low CTT is seen near Kerala and Karnataka coastal areas. The CTT values range between 180 and 190 K over ARBS (Fig. 5(a)). On 15th May, 2021 low CTT is seen near Karnataka and Kerala coastal areas. The CTT values range between 180 and 190 K over ARBS (Fig. 5(b)). On 16th May, 2021 low CTT is seen near Maharashtra coastal areas. The CTT values range between 180 and 190 K over ARBS (Fig. 5(c)). On 17th May, 2021 very low CTT is seen near Gujarat coastal areas. The CTT values range between 180 and 200 K over ARBS (Fig. 5(d)). On 18th May, 2021 the CTT are higher near Gujarat. The CTT values range between 200 and 210 K over ARBS (Fig. 5(e)). On 19th May, 2021 the CTT values are seen increased near Gujarat and Maharashtra coastal areas over ARBS (Fig. 5(f)). These threshold values of CTT are indicating the peak activity of convection that has been discussed in a previous study by Umakanth et al. (2021).
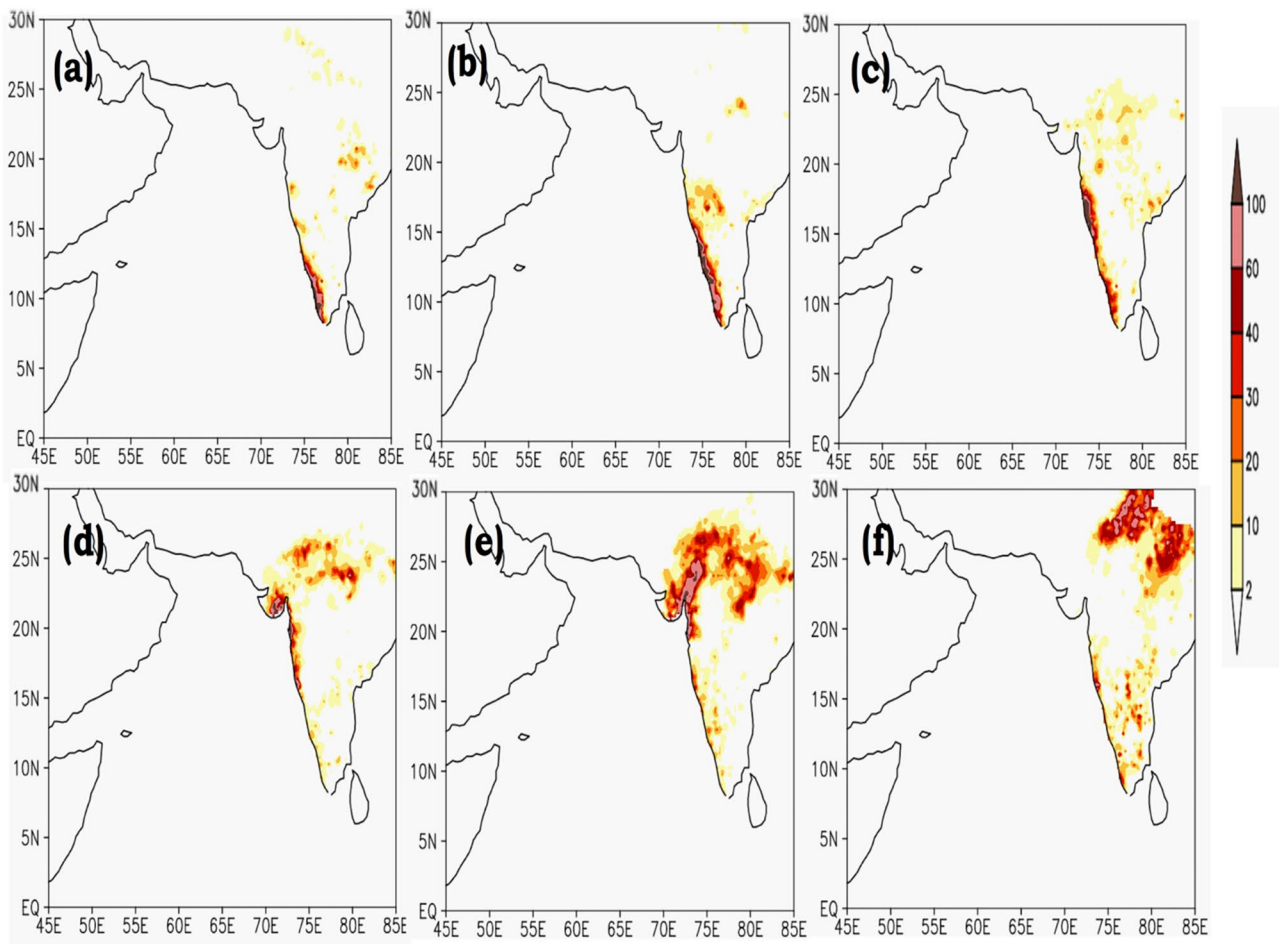

Fig. 4 Spatial distribution of daily IMD rainfall during **a** May 14th, 2021, **b** May 15th, 2021, **c** May 16th, 2021, **d** May 17th, 2021, **e** May 18th, 2021, **f** May 19th, 2021
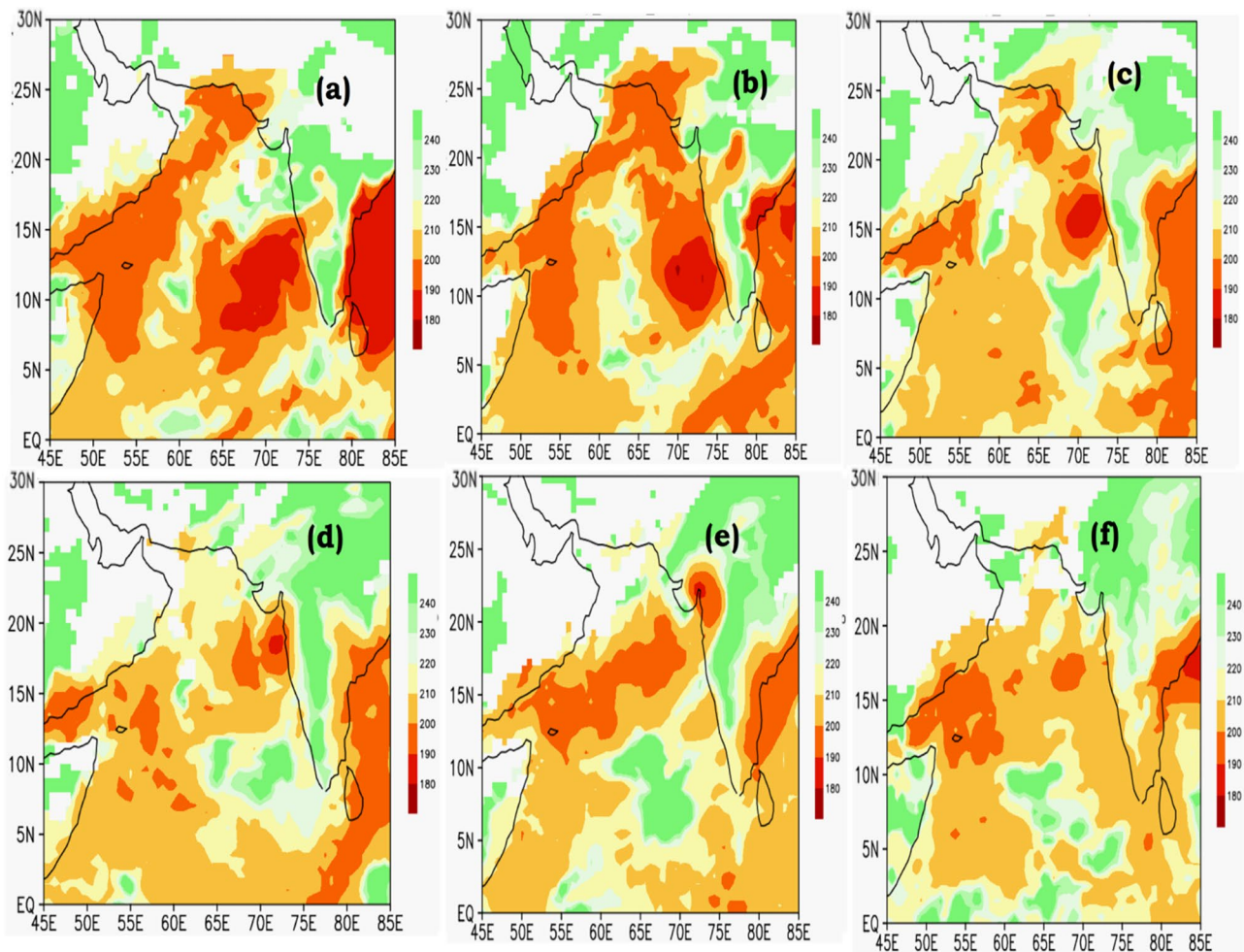
Fig. 5 Spatial distribution of WRF simulated mean daily cloud top temperature during **a** May 14th, 2021, **b** May 15th, 2021, **c** May 16th, 2021, **d** May 17th, 2021, **e** May 18th, 2021, **f** May 19th, 2021

Discussion of SST, SLP, TPW and Wind Vectors with Cyclone Tauktae

Figure 6 shows the simulated SST pattern across the Arabian Sea region from May 14th to 19th, 2021. SST readings in the ARBS region range from 30 to 31 degrees Celsius on May 14th, 2021 (Fig. 6(a)). SST readings in the ARBS region on the 15th of May, 2021 vary from 29.5 to 31 °C (Fig. 6(b)). On 16th May, 2021, the high SST is seen near Maharashtra coastal areas. The SST values range between 30 and 31 °C over ARBS (Fig. 6(c)). On 17th May, 2021, high SST values are seen near Gujarat coastal areas. Over ARBS, the SST values range from 30.5 to 31.1 °C (Fig. 6(d)). On 18th May, 2021, the SST is relatively lesser near Gujarat. The SST values range between 30 and 30.5 °C over ARBS (Fig. 6(e)).

On 19th May, 2021, the SST values are seen decreased near Gujarat and Maharashtra coastal areas over ARBS (Fig. 6(f)). Figure 7(a-f) shows the MERRA2 (Observation) SST pattern across the Arabian Sea region from May 14th to 19th, 2021. SST values in the ARBS region range from 29 to 31.5 degrees Celsius on May 14th, 2021 (Fig. 7(a)). SST values in the ARBS region on the 15th of May, 2021 vary from 29.5 to 31.5 °C (Fig. 7(b)). On 16th May, 2021, the SST values range between 29.5 and 31.5 °C near Maharashtra coastal region (Fig. 7(c)). On 17th May, 2021, the SST values range from 29.5 to 30.5 °C (Fig. 7(d)). On 18th and 19th May, 2021, the SST is relatively lesser near Gujarat as seen in Fig. 7(e-f). On the 17th May, 2021 model simulated SST values showed higher values than observation. These results also corroborate with the previous studies by Reddy
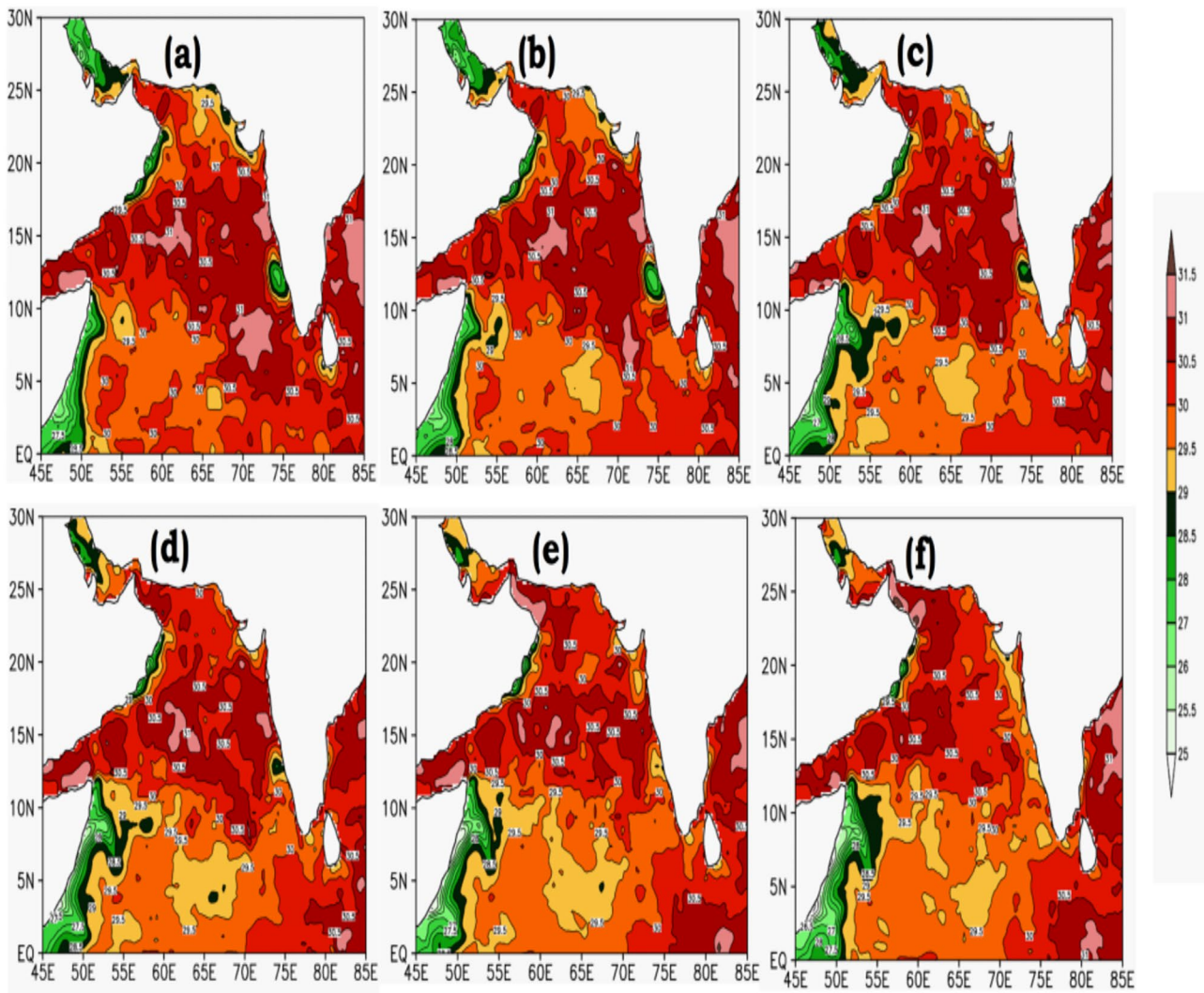
Fig. 6 Spatial distribution of WRF simulated mean daily sea surface temperature during **a** May 14th, 2021, **b** May 15th, 2021, **c** May 16th, 2021, **d** May 17th, 2021, **e** May 18th, 2021, **f** May 19th, 2021

et al. (2023) showing that high SST values from Morrison scheme has been a good precursor for convective instability.

Figure 8 shows the simulated SLP (Shaded) and winds (Vectors) pattern across the Arabian Sea region from May 14th to 19th, 2021. On 14th May, 2021, the SLP values are low near Lakshadweep islands in ARBS. The SLP values drops from 1003hpa to 998hpa over ARBS region. The wind vectors represent that the westerly winds are accumulated around the low pressure area and they move with a speed of nearly 10m/s (Fig. 8(a)). On 15th May, 2021, the SLP values are low near Kerala coast in ARBS. The SLP values drops from 998hpa to 987hpa over ARBS region. According to the

wind vectors (Fig. 8(b)), the low pressure area is surrounded by strong winds that are moving at a speed of 20 m/s. On 16th May, 2021, the SLP values are low near Maharashtra and Karnataka coasts in ARBS. The SLP values drops from 993hpa to 987hpa over ARBS region. According to the wind vectors (Fig. 8(c)), there are strong winds near the low pressure with a speed of 25 m/s. On 17th May, 2021, the SLP values are low near Maharashtra and Gujarat coasts in ARBS. The SLP values drops from 990hpa to 984hpa over ARBS region. According to the wind vectors (Fig. 8(d)), high winds with a speed of 20 m/s have been seen in the area surrounding the low pressure. On 18th May, 2021, the SLP values are
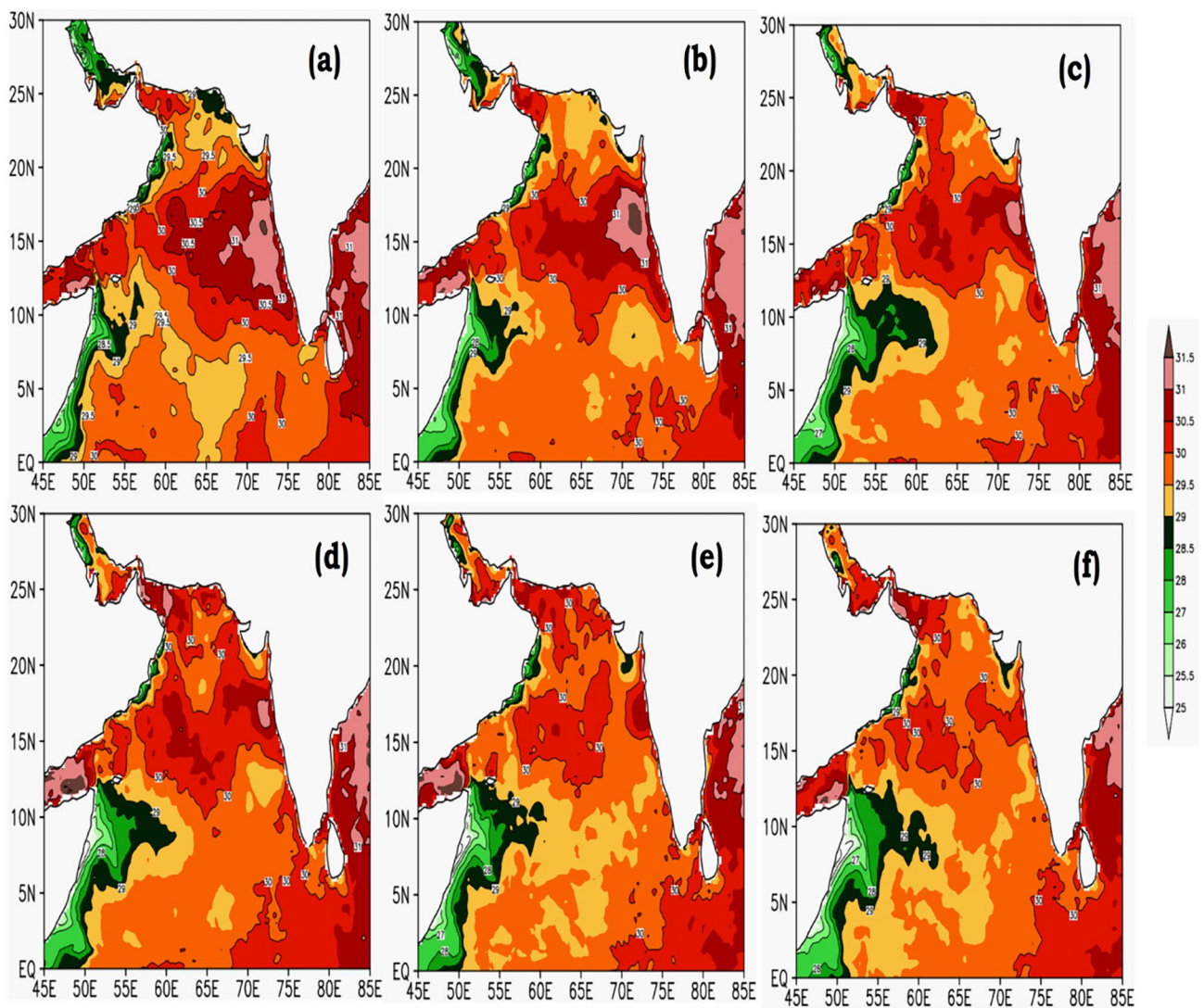
Fig. 7 Spatial distribution of MERRA2(Observation) mean daily sea surface temperature during **a** May 14th, 2021, **b** May 15th, 2021, **c** May 16th, 2021, **d** May 17th, 2021, **e** May 18th, 2021, **f** May 19th, 2021

low near Gujarat coast and land area in ARBS. The cyclone made landfall on 18th. The SLP values drops from 990hpa to 980hpa over ARBS region. According to the wind vectors (Fig. 8(e)), the low pressure area is surrounded by strong winds that are moving at a speed of 20 m/s. On 19th May, 2021, the SLP values are low near Gujarat and Rajasthan area over land. The cyclone made landfall on 18th. So on 19th, the SLP values starts increasing from 992hpa to 998hpa over Gujarat region. The wind vectors indicate that speed of the winds is decreased to 10 m/s (Fig. 8(f)). Figure 9 shows the MERRA2 (Observation) SLP (Shaded) and winds (Vectors) pattern across the Arabian Sea region from May 14th to

19th, 2021. On 14th May, 2021, the SLP values are low near Kerala coastal region in ARBS. The SLP values drops from 1000hpa to 998hpa over ARBS region. The wind vectors represent that the westerly winds are accumulated around the low pressure area and they move with a speed of nearly 10m/s (Fig. 9(a)). On 15th May, 2021, the SLP values are low near Southern Karnataka coast in ARBS. The SLP values drops from 998hpa to 992hpa over ARBS region. According to the wind vectors (Fig. 9(b)), the low pressure area is surrounded by strong winds that are moving at a speed of 20 m/s. On 16th May, 2021, the SLP values are low near Maharashtra coast in ARBS. The SLP values drops from
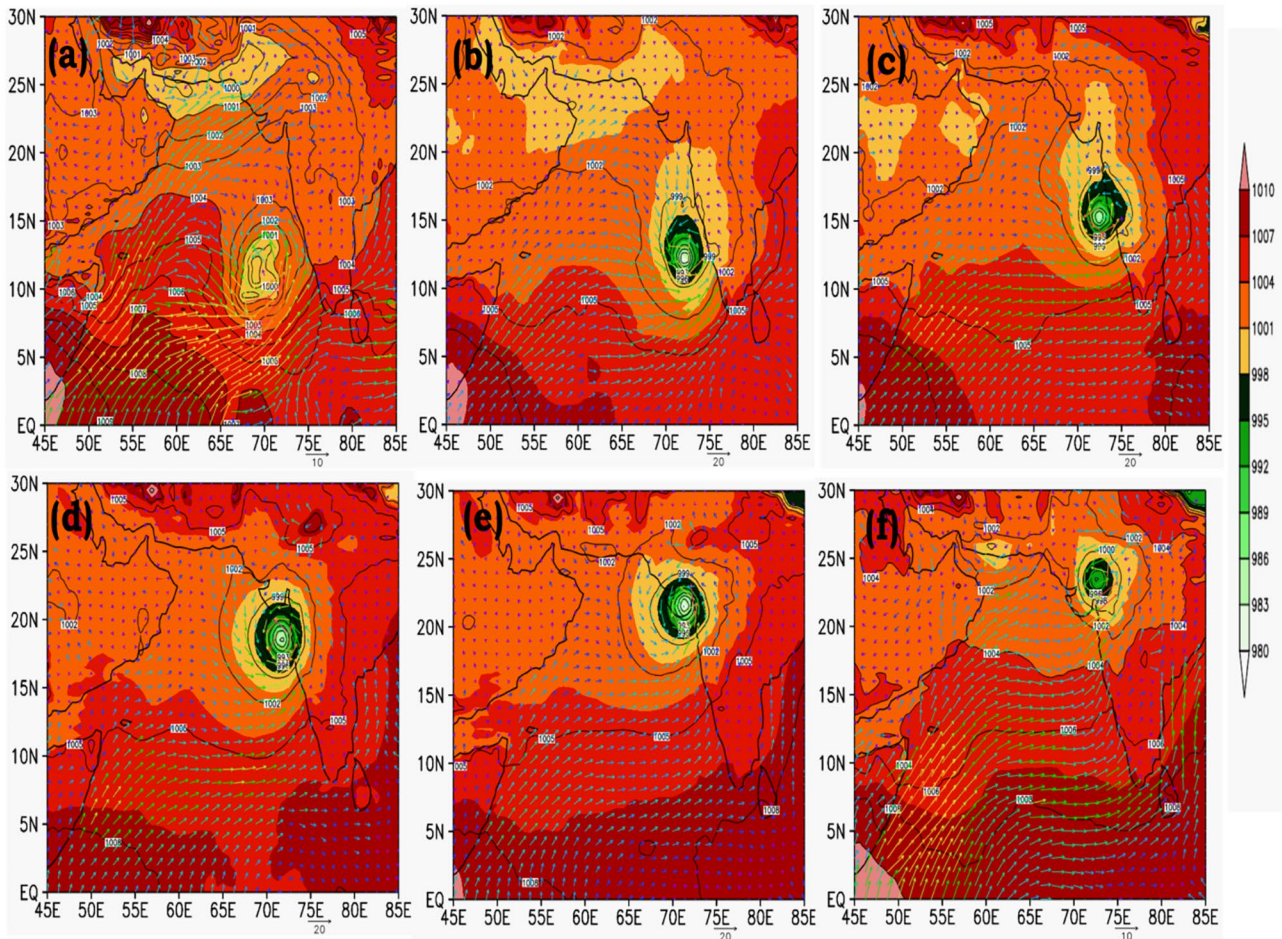
Fig. 8 Spatial distribution of WRF simulated mean daily sea level pressure (shaded) and Wind vectors during **a** May 14th, 2021, **b** May 15th, 2021, **c** May 16th, 2021, **d** May 17th, 2021, **e** May 18th, 2021, **f** May 19th, 2021

993hpa to 989hpa over ARBS region (Fig. 9(c). On 17th May, 2021, the SLP values are low near Gujarat coasts in ARBS. The SLP values drops from 990hpa to 986hpa over ARBS region. According to the wind vectors (Fig. 9(d)), high winds with a speed of 20 m/s have been seen in the area surrounding the low pressure. On 18th May, 2021, the SLP values drops from 998hpa to 992hpa over Gujarat (Fig. 9(e)). On 19th May, 2021, the SLP values varied from 1001hpa to 998hpa over Gujarat region (Fig. 9(f)). This result has been matching with the previous study by Atkinson and Holliday (1977) showing that low SLP values and high wind speeds are a good indication for severe unstable atmosphere in the cyclone occurrence region.

Figure 10 shows the simulated TPW (Shaded) and divergence (Contour) pattern across the Arabian Sea region from May 14th to 19th, 2021. On 14th May, 2021, the TPW values are high near Lakshadweep islands and Kerala coast

in ARBS. The TPW values lie from 60 to 70 mm over ARBS region. The divergence values range between -0.3 and -0.9 favouring the moisture accumulation across the ARBS (Fig. 10(a)). On 15th May, 2021, the TPW values are high near Kerala and Karnataka coasts in ARBS. The TPW values over the ARBS region vary from 60 to 80 mm. According to ARBS (Fig. 10(b)), the divergence values, which range from -0.5 to -1.0, support moisture accumulation along the coasts of Kerala and Karnataka. On 16th May, 2021, the TPW values are high near Maharashtra and Karnataka coasts in ARBS. Over the ARBS region, the TPW values range from 60 to 80 mm. According to ARBS, divergence values between -0.2 and -0.5 support moisture accumulation along the beaches of Maharashtra and Karnataka (Fig. 10(c)). On 17th May, 2021, the TPW values are high near Maharashtra and Gujarat coasts in ARBS. The TPW values range from 50 to 80 mm over ARBS region.
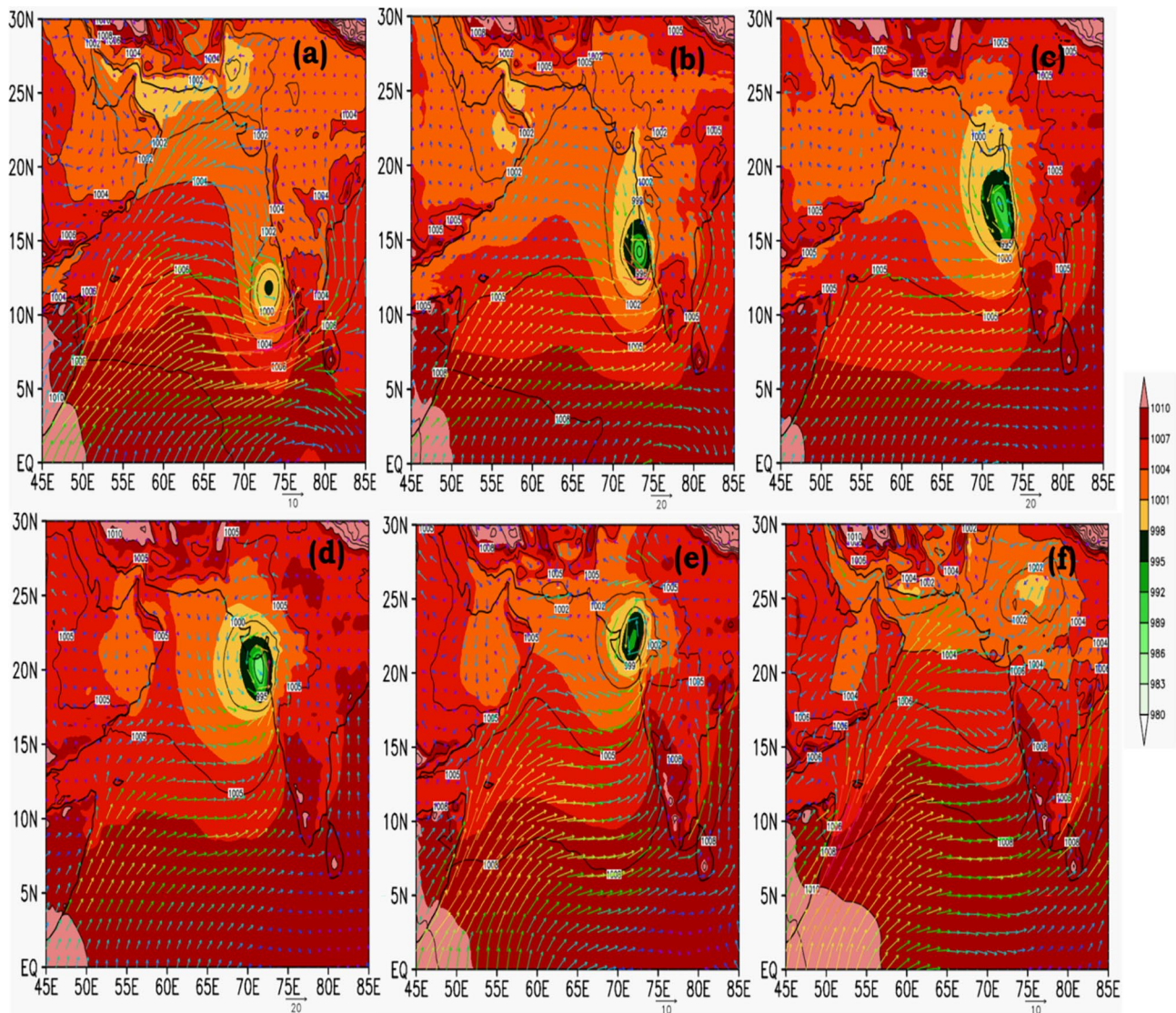
Fig. 9 Spatial distribution of MERRA2(Observation) mean daily sea level pressure (shaded) and Wind vectors during **a** May 14th, 2021, **b** May 15th, 2021, **c** May 16th, 2021, **d** May 17th, 2021, **e** May 18th, 2021, **f** May 19th, 2021

The divergence values range between -0.2 and -0.5 favouring the moisture accumulation across the Maharashtra and Gujarat coasts in ARBS (Fig. 10(d)). On 18th May, 2021, the TPW values are high near Gujarat coast and land area in ARBS. The TPW values lies from 60 to 82 mm over ARBS region. The divergence values range between -0.4 and -1.0 favouring the moisture accumulation across the Gujarat coast (Fig. 10(e)). On 19th May, 2021, the TPW values are high near Gujarat and Rajasthan area over land. The cyclone made landfall on 18th. So on 19th, the TPW values starts decreasing from 82 to 50 mm over Gujarat region. The

divergence values range between -0.1 and -0.5 across the ARBS (Fig. 10(f)). Figure 11 shows the MERRA2 (Observation) TPW (Shaded) and divergence (Contour) pattern across the Arabian Sea region from May 14th to 19th, 2021. The WRF simulated TPW values showed higher values than MERRA2 values. The WRF simulations showed strong convergence than MERRA2 over the ARBS (Figs. 10 and 11). This result has been coinciding with the previous studies by Umakanth et al. (2021) and Takakura et al. (2018) showing that the TPW values tend to increase in an extreme unstable atmosphere leading to a high rainfall occurrence.
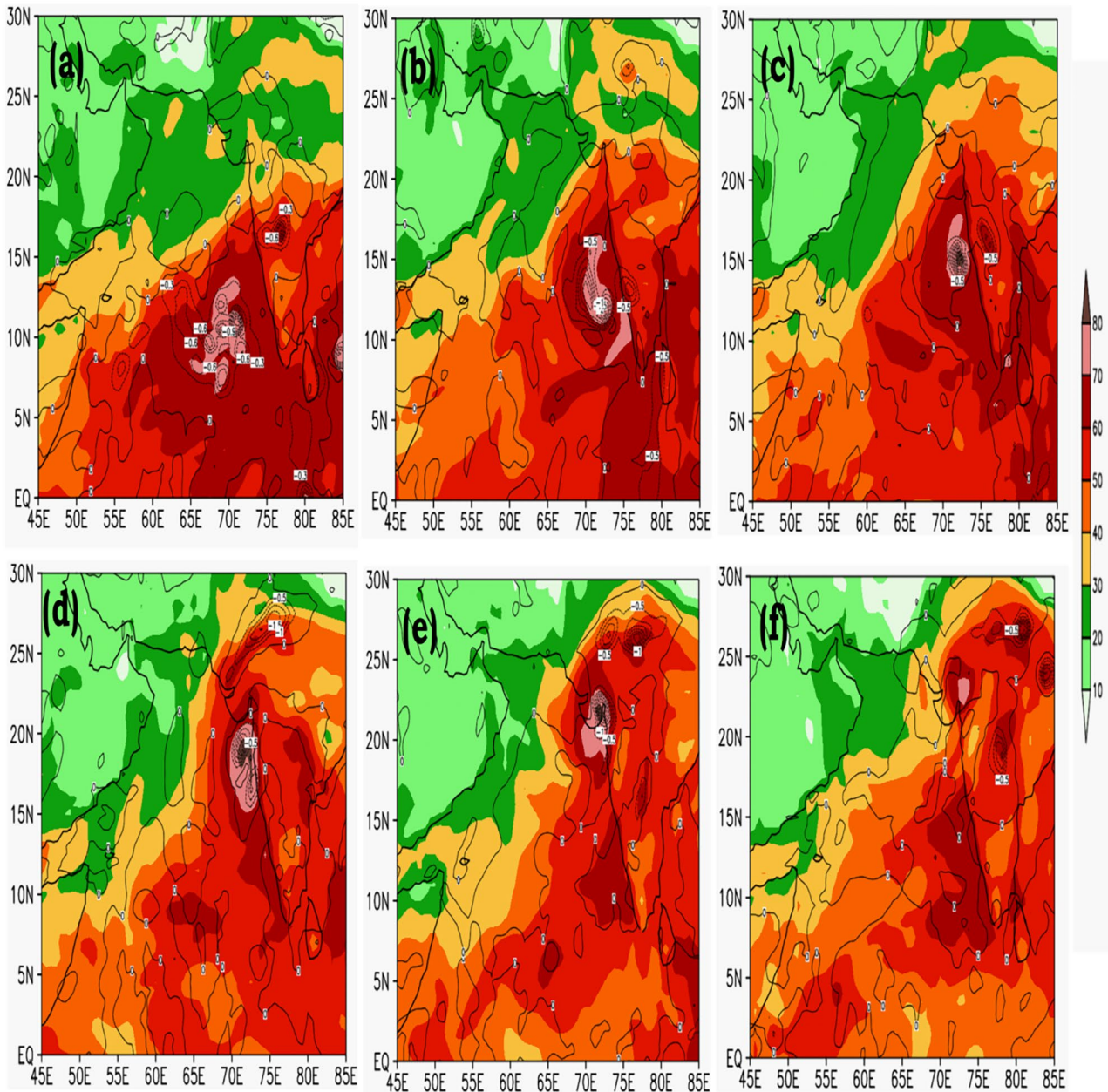
Fig. 10 Spatial distribution of WRF simulated mean daily TPW (shaded) and divergence (contour) during **a** May 14th, 2021, **b** May 15th, 2021, **c** May 16th, 2021, **d** May 17th, 2021, **e** May 18th, 2021, **f** May 19th, 2021

Discussion of CAPE, CIN and LI with Cyclone Tauktae

Figure 12 shows the simulated CAPE pattern across the Arabian Sea region from May 14th to 19th, 2021. On May 14th, 2021, CAPE levels in the ARBS region range from 500 to 1500 J/kg (Fig. 12(a)). On May 15, 2021, CAPE values in the ARBS region range from 1000 to 2000 J/kg (Fig. 12(b)). On May 16, 2021, a high CAPE is noted close to the coastal regions of Maharashtra. Over ARBS, CAPE values range from 1500 to 2000 J/kg (Fig. 12(c)). High CAPE values were observed around Gujarat coastal areas on May 17th, 2021. According to Fig. 12(d), CAPE values over ARBS range from 1000 to 2500 J/kg. On May 18, 2021, the CAPE is larger near Gujarat. According to Fig. 12(e), CAPE values over ARBS range from 1000 to 1500 J/kg. CAPE values along Gujarat and Maharashtra coastal areas dropped over
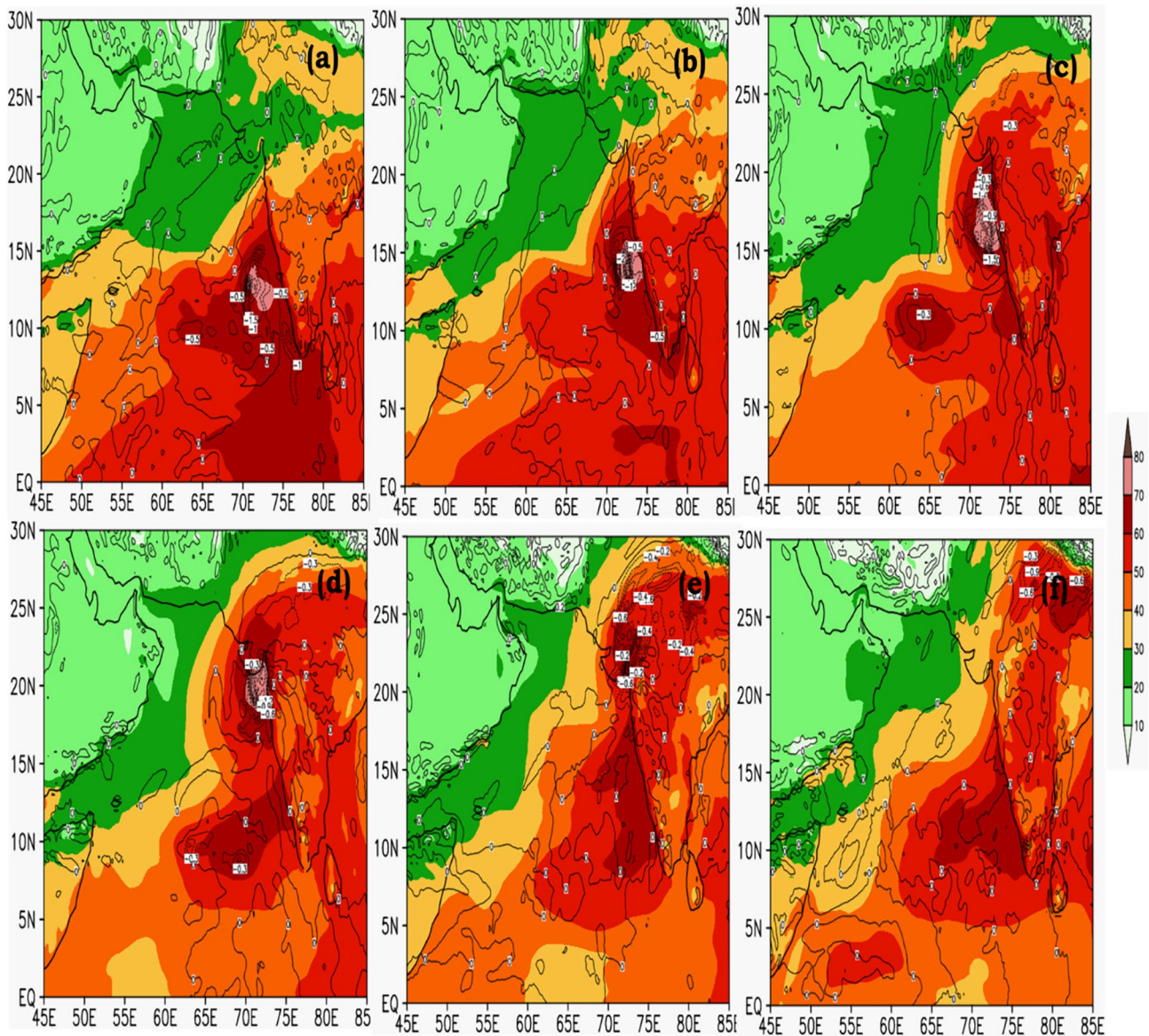
Fig. 11 Spatial distribution of MERRA2(Observation) mean daily TPW (shaded) and divergence (contour) during **a** May 14th, 2021, **b** May 15th, 2021, **c** May 16th, 2021, **d** May 17th, 2021, **e** May 18th, 2021, **f** May 19th, 2021

ARBS on May 19th, 2021 (Fig. 12(f)). From this Fig. 12, it can be seen that the start of the severe cyclonic downpour is accompanied by a rise in the CAPE value, since it is well known that the cyclone's eye is essentially encircled by huge thunderstorms. A high CAPE value suggests a high likelihood of severe weather, such as cyclones and thunderstorms. Understanding and forecasting the characteristics of cyclones depend heavily on the WRF-simulated CAPE parameter (Molinari et al. 2012). Tables 3, 4, and 5 illustrates that the Morrison simulated CAPE had a strong

correlation, low RMSE, and BIAS in connection to the MERRA2 observations.

Figure 13 shows the simulated LI pattern across the Arabian Sea region from May 14th to 19th, 2021. On May 14th, 2021, the LI values in the ARBS region range from -4 to -2K (Fig. 13(a)). On the 15th of May, 2021, the LI values in the ARBS region vary from -4 to -2K (Fig. 13(b)). The low LI is visible near Maharashtra coastal areas on May 16th, 2021. Over ARBS, LI values range from -2 to -1K (Fig. 13(c)). The LI values are seen around Gujarat coastal areas on May 17th,
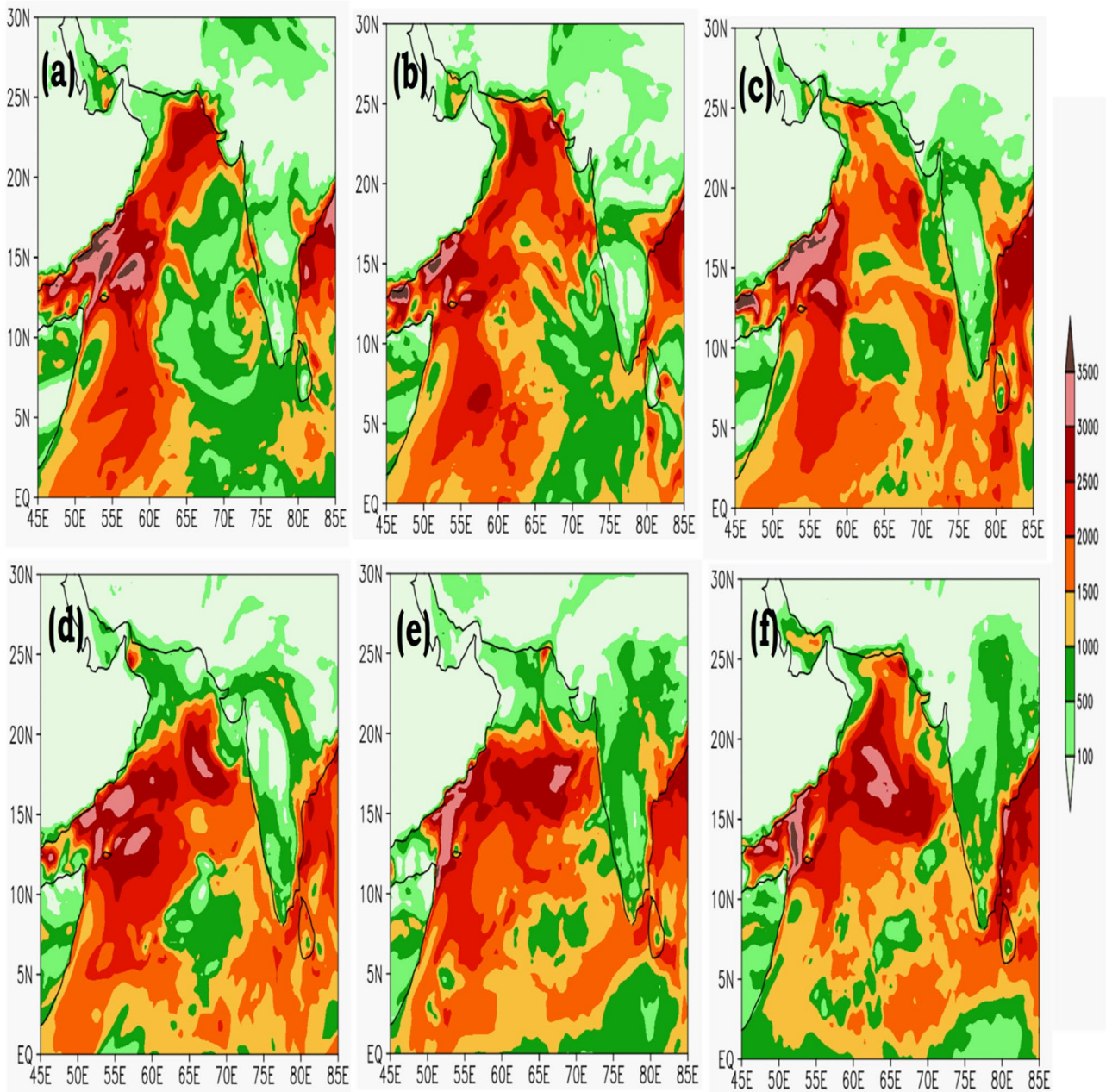
Fig. 12 Spatial distribution of WRF simulated mean daily CAPE during **a** May 14th, 2021, **b** May 15th, 2021, **c** May 16th, 2021, **d** May 17th, 2021, **e** May 18th, 2021, **f** May 19th, 2021

2021. Over ARBS, LI values vary from -1 to 2K (Fig. 13(d)). The LI values near Gujarat are positive on May 18th, 2021. Over ARBS, LI values vary from -2 to 2K (Fig. 13(e)). On the 19th of May, 2021, the LI values near the Gujarat and Maharashtra coasts plummeted over ARBS (Fig. 13(f)). The behaviour of cyclones can be understood and predicted using LI. A negative LI may point to an unstable environment that

is favourable for convection, which is essential for cyclogenesis, developing before a cyclone occurs. A cyclone's continuous convective activity, which is required for the cyclone to strengthen, can be indicated by a consistently negative LI in some areas of the storm during its development phase. The eyewall and inner rainbands of a mature cyclone are two structurally significant zones of heavy convection that
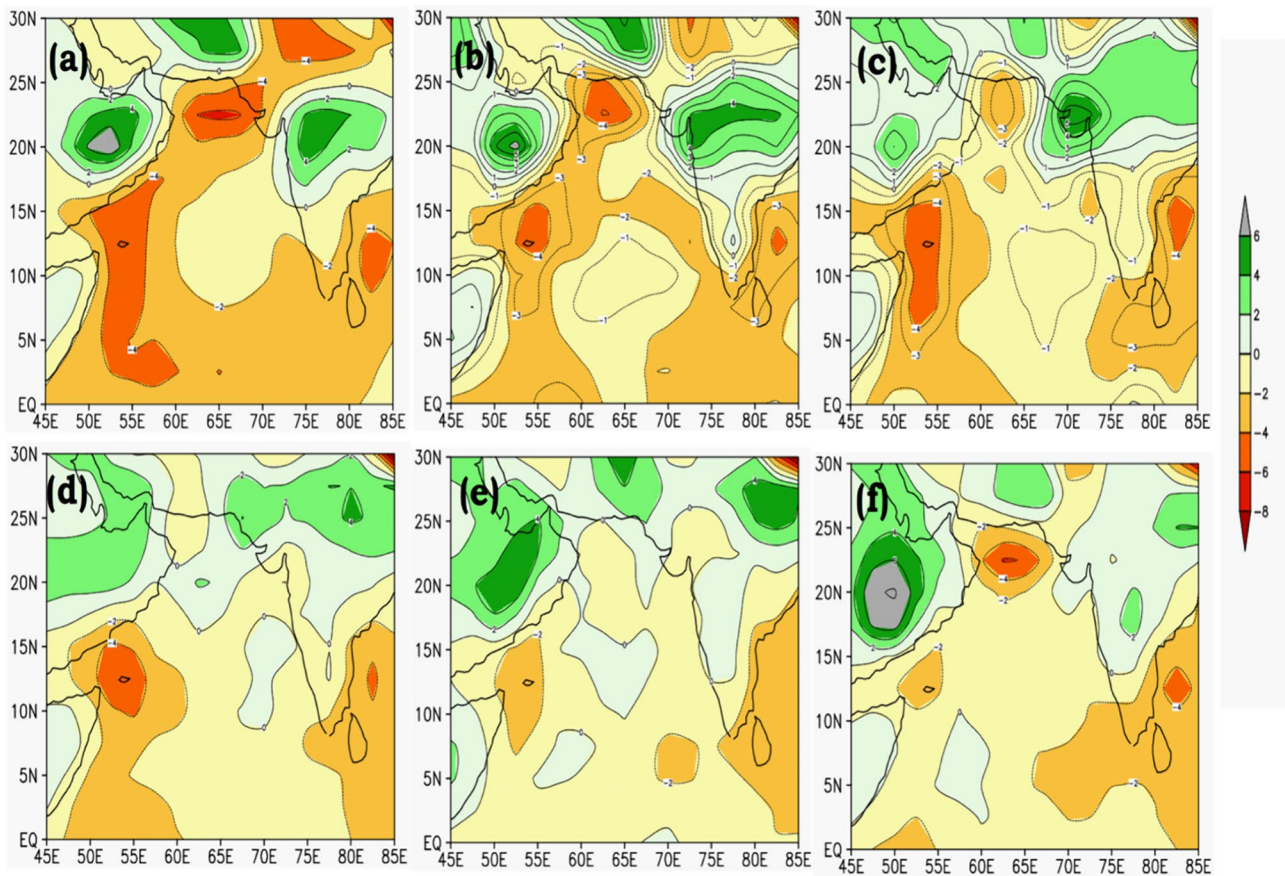
Fig. 13 Spatial distribution of WRF simulated mean daily LI during **a** May 14ᵗʰ, 2021, **b** May 15ᵗʰ, 2021, **c** May 16ᵗʰ, 2021, **d** May 17ᵗʰ, 2021, **e** May 18ᵗʰ, 2021, **f** May 19ᵗʰ, 2021

can be located with the aid of the LI. According to Peppler (1988), these regions usually have extremely negative LI values. The stability and convective potential inside a cyclone are largely dependent on the WRF-simulated LI parameter. We can see from Tables 3–5 that the Morrison simulated LI had low RMSE, BIAS, and strong correlation with the MERRA2 data.

Figure 14 shows the simulated CIN pattern across the Arabian Sea region from May 14ᵗʰ to 19ᵗʰ, 2021. CIN values in the ARBS region range between -25 and -200 J/kg from May 14ᵗʰ to 19ᵗʰ, 2021 (Fig. 14(a-f)). This is a strong indicator of severe atmospheric instability. CIN represents the suppression of cyclone potential. Higher CIN values shows the presence of a stable layer that hinders convection by preventing air parcels from rising freely. Convection can start more readily when the CIN value is low, which indicates less resistance to upward motion. A crucial measure for comprehending the suppression and convection initiation of cyclones is WRF-simulated CIN. To improve forecasts

and comprehend the mechanisms of cyclone genesis and intensification, precise modelling and validation against observational data are crucial (Parker 2002). Morrison's simulated CIN demonstrated a high degree of correlation, low RMSE, and BIAS with MERRA2 measurements, as shown in Tables 3–5.

Comparison of WRF and MERRA2 Results on May 17ᵗʰ, 2021

As per the IMD report, the cyclone made landfall in night time (15UTC) of 17ᵗʰ May, 2021. Figure 15(a) shows the WRF model simulated CAPE pattern across the Arabian Sea region at 06UTC on May 17ᵗʰ, 2021. High CAPE values were seen near the Gujarat and Maharashtra coasts on May 17ᵗʰ, 2021. The CAPE values nearly approached 3000 J/kg, indicating the extreme convection activity over the region of occurrence (Fig. 15(a)). The WRF model showed higher CAPE values than the MERRA2 CAPE data. The convective severity of the storm was also indicated by the WRF model simulated
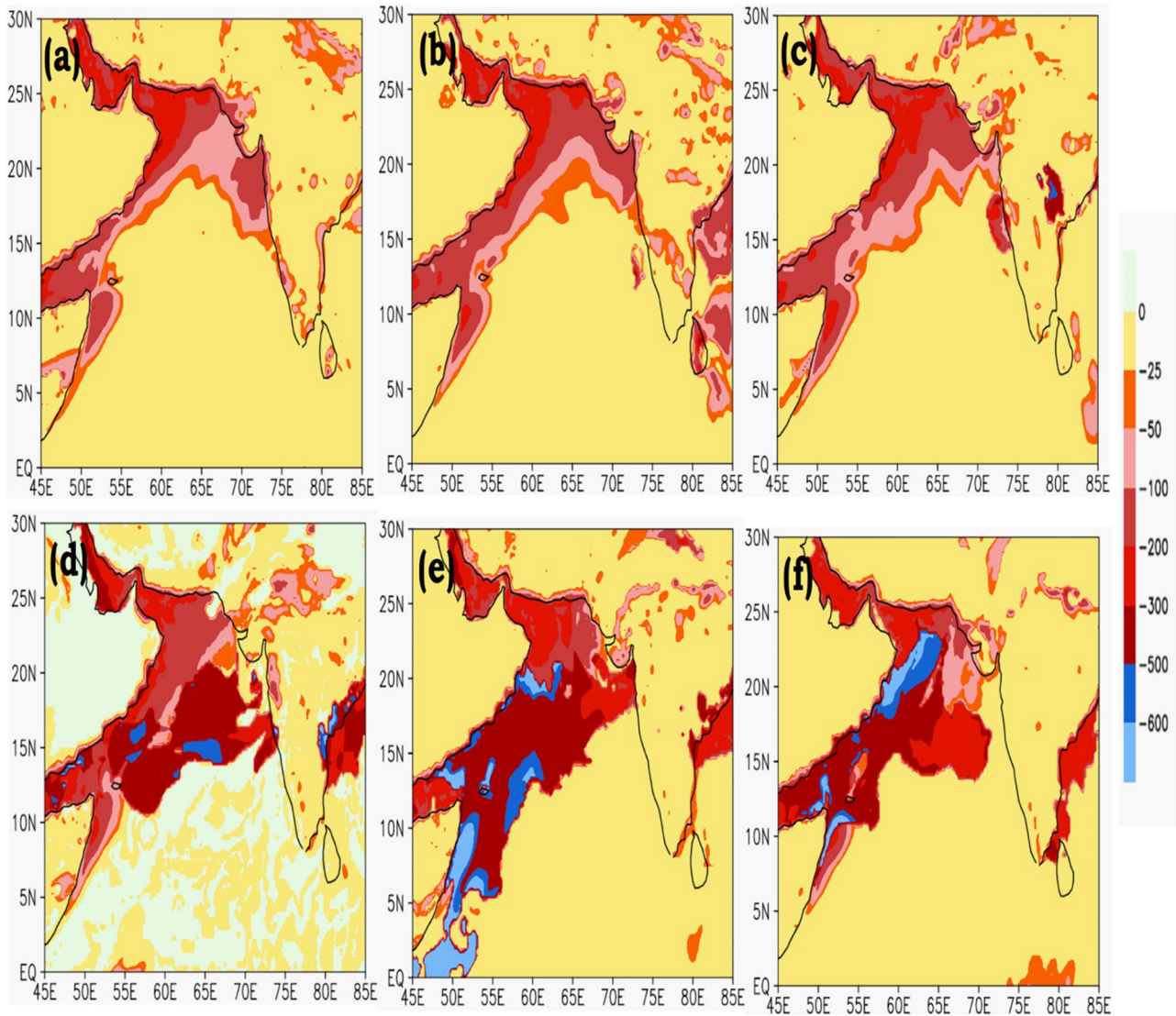
Fig. 14 Spatial distribution of WRF simulated mean daily CIN during **a** May 14th, 2021, **b** May 15th, 2021, **c** May 16th, 2021, **d** May 17th, 2021, **e** May 18th, 2021, **f** May 19th, 2021

CIN values. The threshold values varied from -50 to -200 (Fig. 15(b)). The WRF model simulated LI values ranging between -6K and -4K indicating severe unstable atmosphere that is conducive for the development of severe convection activity (Fig. 15c). We have also tried to look at the wind gust in the WRF model simulation. High wind gust values were noticed near Gujarat coast. Wind gust values almost lie between 20 and 40 m/s indicating the severity of cyclone (Fig. 15(d)). The complex reflectivity (~ 10 to 35) & SRLH

(~ 150 to 300) showed the severity of the cyclone occurrence at 06UTC (Fig. 16(a) & (b)). The model simulation results showed high relative humidity (60 to 85) values at the coast of Gujarat (Fig. 16(c)). Lower dew point depression values signify a very moist atmosphere around the convection occurrence. These high relative humidity values and low dew point depression values will tend to intensify the convection process at the coastal regions leading to severe damage (Wu et al. 2015 and Srinivas et al. 2018). Geo-potential height (GPH) helps
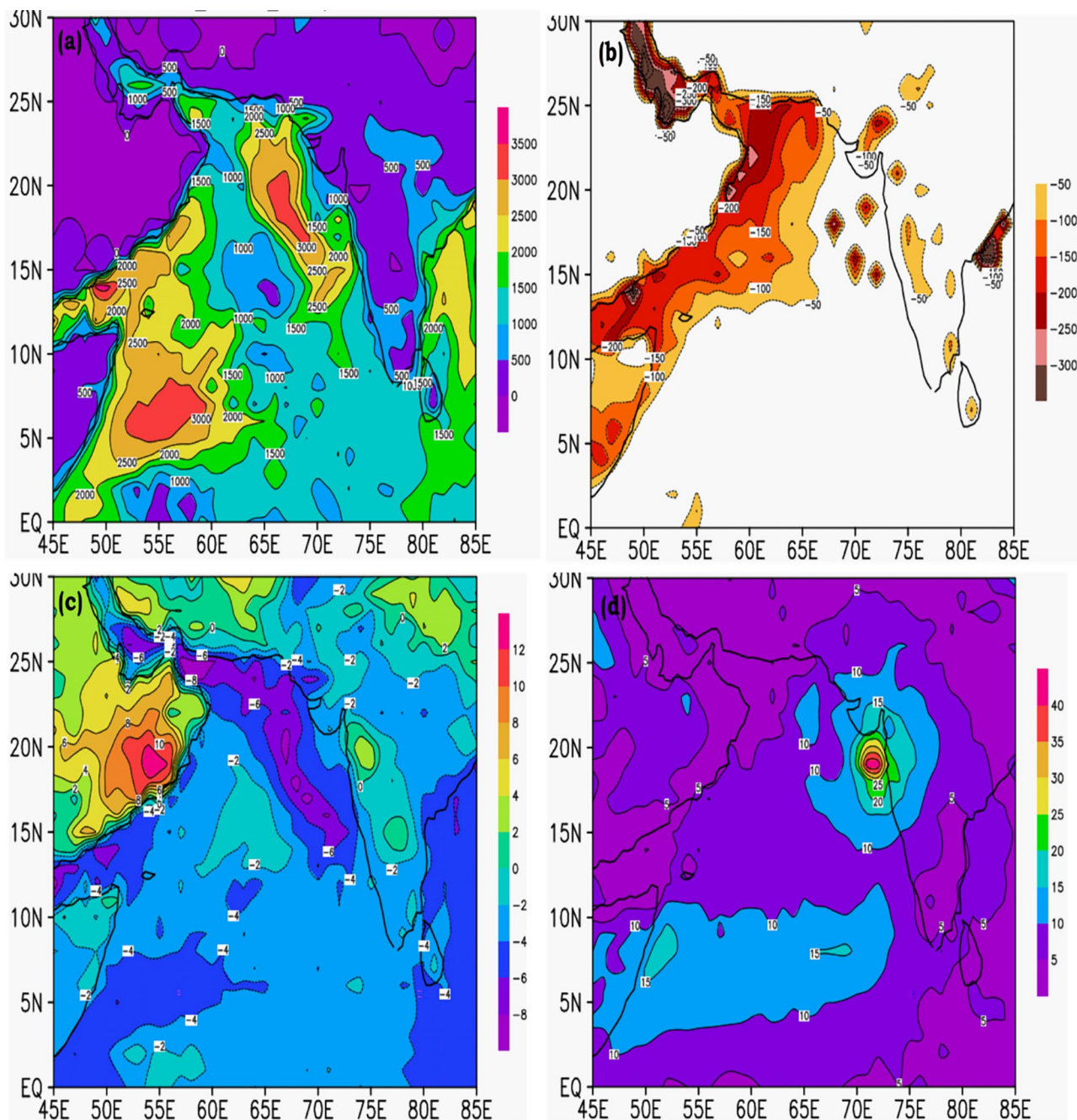
Fig. 15 Spatial distribution of WRF simulated **a**. CAPE, **b**. CIN, **c**. LI and **d**. wind gust parameters at 06UTC on May 17th, 2021

us to understand the height of the pressure surface beyond the mean sea level. The model simulation results showed lower GPH values near Gujarat coast (Fig. 16(d)). Lower GPH

values signifies high availability of warm air (Moore and Dixon 2015). The simulated results of WRF Morrison scheme were able to emphasize the convective features of the cyclone.
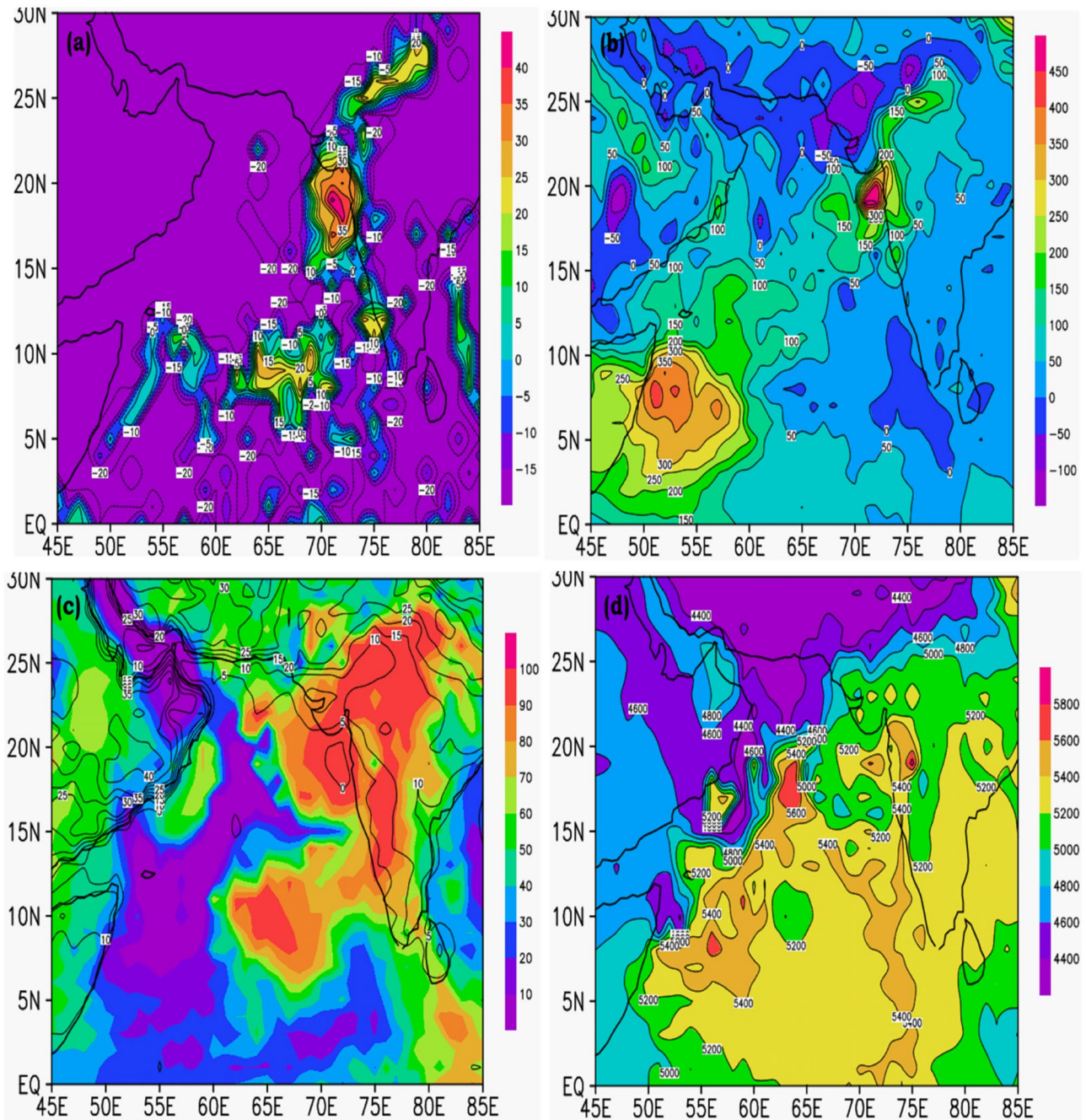
Fig. 16 Spatial distribution of WRF simulated **a**. composite reflectivity, **b**. SRLH, **c**. relative humidity (shaded) and dew point depression (contour), **d**. geo-potential height parameters at 06UTC on May 17th, 2021

Conclusions

An attempt has been made in this paper to examine the tropical cyclone Tauktae over the Arabian Sea with the help of WRF microphysics model during May 14-19, 2021. Three microphysics schemes (Morrison, Thompson, Lin) were tested and their performances were evaluated by computing various convective related parameters with observational data. Morrison scheme produced the best results for assessment of convective parameters. Thompson was the second best scheme, while Lin showed the least correlation for all parameters.

The Morrison simulated results emphasize that high rainfall over Gujarat's coastal areas on May 17th, 2021.

Thermodynamic stability parameters computed from Morrison simulated WRF model vertical temperature and humidity profiles have shown rapid changes, at least from 10 hrs before the land fall, that favour deep convection. Convective parameters (CAPE, CIN, LI, TPW) along with CTT have been found to be useful in the assessment of cyclone.

Over ARBS, CTT values range from 180 to 200 K at 06 UTC on May 17th, 2021. This is 10 hours before the landfall. The SLP values drop from 990hpa to 984hpa and winds of 20 m/s have been detected near the low pressure. High TPW values (50-80 mm) and negative divergence values (-0.2 to -0.5) over ARBS are favoring moisture accumulation along the beaches of Maharashtra and Gujarat. High SST values were seen around Gujarat coastal areas on May 17th, 2021. Over ARBS, SST values vary from 30.5 to 31.1 °C. High CAPE (1500-2500 J/Kg) and low LI (2 to -1 K) over ARBS indicated the instability over Gujarat coast. Overall this analysis indicated that the sensitivity of the simulated cyclone Tauktae to Morrison microphysics scheme is due to the variations in the convective parameters.

The Morrison cumulus scheme exhibits as a reliable choice for rainfall simulation over ARBS. These convective parameters were in good agreement with MERRA2 calculated indices, indicating rapid changes in the parameters at 6-hr lead time, emphasizing the use of WRF model in the prediction of cyclone.

Author Contributions Nandivada Umakanth: Writing – review & editing, Writing – original draft, Visualization, Validation, Methodology, Formal analysis, Data curation, Conceptualization Prathipati Vinay Kumar: Writing – original draft, Software, Methodology, Data curation. Rupraj Biswasharma: Software, Methodology, Formal analysis, Data curation. Myla Chimpiri Rao, Rajesh Gogineni: Writing – review & editing, Writing – original draft, Supervision, Investigation. Shaik Hasane Ahammad: Writing – review & editing, Writing – original draft, Supervision, Investigation.

Data Availability The IMD, MERRA2 and NCEP FNL datasets are used in this study's analysis. The NCEP FNL data was available at https://rda.ucar.edu/datasets/ds083.2/. Data from the Modern Era Retrospective Analysis for Research and Application (MERRA) project were collected using https://disc.gsfc.nasa.gov/datasets?project=MERRA-2. The IMD data is available at the link https://www.imdpune.gov.in/cmpg/Griddata/Rainfall_25_NetCDF.html.

Declarations

Ethics Approval and Consent to Participate The authors have stated that they do not have any competing interests in the publication of this work.

Human and Animal Ethics Not Applicable.

Consent for Publication Each author grants permission for the data and findings from this work to be published in "Thalassas: An International Journal of Marine Sciences" so that anyone can access and utilise the information with the appropriate acknowledgment.

The Role of the Financing Sources This paper has no funding sources specified.

Competing Interests The authors declare no competing interests.

References

Ali MM, Kashyap T, Nagamani PV (2013) Use of sea surface temperature for cyclone intensity prediction needs a relook. Trans Am Geophys Union 94:177–178

Atkinson GD, Holliday CR (1977) Tropical cyclone minimum sea level pressure/maximum sustained wind relationship for the western North Pacific. Mon Weather Rev 105(4):421–427

Balaguru Karthik, Sourav Taraphdar L, Leung Ruby, Gregory RF (2014) Increase in the intensity of postmonsoon Bay of Bengal tropical cyclones. Geophys Res Lett 41(10):3594–3601

Biswasharma R, Umakanth N, Ao Imlisunup, Longkumar Imolemba, Rao KMM, Pawar SD, Gopalakrishnan V, Sharma S (2024) Sensitivity Analysis of Microphysics and Cumulus Schemes in the WRF Model in Simulating Extreme Rainfall Events over the Hilly Terrain of Nagaland. Preprints. https://doi.org/10.2139/ssrn.4661662

Camargo SJ, Matthew CW, Adam HS (2009) Diagnosis of the MJO modulation of tropical cyclogenesis using an empirical index. J Atmos Sci 66(10):3061–3074

Camargo SJ, Adam HS, Anthony GB, Philip JK (2010) The influence of natural climate variability on tropical cyclones, and seasonal forecasts of tropical cyclone activity. In Global perspectives on tropical cyclones: From science to mitigation 1(10):325–360. https://doi.org/10.1142/9789814293488_0011

Carlson TN, Eileen MP, Thomas JS (1990) Remote estimation of soil moisture availability and fractional vegetation cover for agricultural fields. Agric For Meteorol 52(1–2):45–69

Chen R, Zhang W, Wang X (2020) Machine learning in tropical cyclone forecast modeling: A review. Atmosphere 11(7):676

Conte D, Miglietta MM, Levizzani V (2011) Analysis of instability indices during the development of a Mediterranean tropical-like cyclone using MSG-SEVIRI products and the LAPS model. Atmos Res 101(1–2):264–279

Deshpande MS, Pattnaik S, Salvekar PS (2012) Impact of cloud parameterization on the numerical simulation of a super cyclone. Ann Geophys 30(5):775–795

Dunkerton TJ, Montgomery MT, Wang Z (2009) Tropical cyclogenesis in a tropical wave critical layer: easterly waves. Atmos Chem Phys 9(15):5587–5646

Emmanuel R, Deshpande M, Ganadhi MK, Ingle ST (2021) Genesis of severe cyclonic storm Mora in the presence of tropical waves over the North Indian Ocean. Q J R Meteorol Soc 147(738):3017–3031

Galway JG (1956) The lifted index as a predictor of latent instability. Bull Am Meteorol Soc 37(10):528–529

Gelaro RW, Max JS, Todling Ricardo, Molod Andrea, Takacs Lawrence, Cynthia AR (2017) The modern-era retrospective analysis for research and applications, version 2 (MERRA-2). J Clim 30(14):5419–5454

Gogineni R, Sangani DJ (2022) A two-stage PAN-sharpening algorithm based on sparse representation for spectral distortion reduction. Int J Image Graph 22(01):2250007

Gray WM (1968) Global view of the origin of tropical disturbances and storms. Mon Weather Rev 96(10):669–700

Haklander AJ, Delden AV (2003) Thunderstorm predictors and their forecast skill for The Netherlands. Atmos Res 67–68:273–299

Houze RA, Lee WC, Bell MM (2009) Convective contribution to the genesis of hurricane Ophelia (2005). Mon Weather Rev 137(9):2778–2800

Hoyos CD, Paula AA, Peter JW, Judith AC (2006) Deconvolution of the factors contributing to the increase in global hurricane intensity. Science 312(5770):94–97

Johnson NC, Xie Shang-Ping (2010) Changes in the sea surface temperature threshold for tropical convection. Nat Geosci 3(12):842–845

Lin YL, Farley RD, Orville HD (1983) Bulk parameterization of the snow field in a cloud model. J Appl Meteorol Climatol 22(6):1065–1092

Maloney ED, Gettelman Andrew, Yi Ming JDN, Barrie Daniel, Mariotti Annarita, Chen CC (2019) Process-oriented evaluation of climate and weather forecasting models. Bull Am Meteorol Soc 100(9):1665–1686

Manche SS, Nayak RK, Rajesh S, Bothale RV, Chauhan P (2024) Characteristics of mesoscale eddies and their evolution in the north Indian ocean. Prog Oceanogr 221(103213):1–17

Mohan PR, Srinivas CV, Yesubabu V, Baskaran R, Venkatraman B (2018) Simulation of a heavy rainfall event over Chennai in Southeast India using WRF: Sensitivity to microphysics parameterization. Atmos Res 210:83–99

Mohan PR, Srinivas CV, Yesubabu V, Baskaran R, Venkatraman B (2019) Tropical cyclone simulations over Bay of Bengal with ARW model: Sensitivity to cloud microphysics schemes. Atmos Res 230

Mohanty UC, Krishna KO, Pattanayak Sujata, Sinha P (2012) An observational perspective on tropical cyclone activity over Indian seas in a warming environment. Nat Hazards 63:1319–1335

Molinari J, Romps DM, Vollaro D, Nguyen L (2012) CAPE in tropical cyclones. J Atmos Sci 69:2452–2462

Moncrieff MH, Miller MJ (1976) The dynamics and simulation of tropical cumulonimbus and squall lines. Q J R Meteorol Soc 102(432):373–394

Montgomery MT, Davis C, Dunkerton T, Wang Z, Velden C, Torn R, Majumdar S, Zhang F, Smith RK, Bosart L, Bell MM, Haase JS, Heymsfield A, Jensen J, Campos T, Boothe MA (2012) The Pre-depression Investigation of Cloud Systems in the Tropics (PREDICT) experiment: Scientific basis, new analysis tools, and some first results. Bull Am Meteorol Soc 93:153–172

Moore TW, Dixon RW (2015) Patterns in 500 hPa geopotential height associated with temporal clusters of tropical cyclone tornadoes. Meteorol Appl 22(3):314–322

Morrison H, Thompson G, Tatarskii V (2009) Impact of cloud microphysics on the development of trailing stratiform precipitation in a simulated squall line: Comparison of one-and two-moment schemes. Mon Weather Rev 137(3):991–1007

Morrison H, Milbrandt JA, Bryan GH, Ikeda K, Tessendorf SA, Thompson G (2015) Parameterization of cloud microphysics based on the prediction of bulk ice particle properties. Part II: Case study comparisons with observations and other schemes. J Atmos Sci 72(1):312–339

Mukhopadhyay P, Sanjay J, Singh SS (2003) Objective forecast of thundery/non thundery days using conventional indices over three northeast Indian stations. Mausam 54(4):867–880

Nolan DS (2007) What is the trigger for tropical cyclogenesis. Aust Meteorol Mag 56(4):241–266

Pai SD, Sridhar Latha, Rajeevan M, Sreejith OP, Satbhai SN, Mukhopadhyay B (2014) Development of a new high spatial resolution(0.25 X 0.25) long period (1901–2010) daily gridded rainfall data set over India and its comparison with existing data sets over the region. Mausam 65(1):1–18

Parker DJ (2002) The response of CAPE and CIN to tropospheric thermal variations. Quart J Roy Meteorol Soc: J Atmos Sci Appl Meteor Phys Oceanogr 128(579):119–130

Peppler RA (1988) A review of static stability indices and related thermodynamic parameters. Illinois State Water Survey Misc Publ 104(87):1–94. https://www.ideals.illinois.edu/items/49020

Pirro A, Fernando HJS, Wijesekera HW, Jensen TG, Centurioni LR, Jinadasa SUP (2020) Eddies and currents in the Bay of Bengal during summer monsoons. Deep-Sea Res II Top Stud Oceanogr 172

Rajesh G, Babu SC (2012) An efficient and reliable algorithm for the RWA problem in optical WDM networks. Int J Eng Res Technol 1(7):1–3

Raju RM, Nayak RK, Mulukutla S, Mohanty PC, Manche SS, Seshasai MVR, Dadhwal VK (2022) Variability of the thermal front and its relationship with Chlorophyll-a in the north Bay of Bengal. Reg Stud Mar Sci 56:102700

Rasmussen EN, Blanchard DO (1998) A baseline climatology of sounding-derived supercell and tornado forecast parameters. Weather Forecast 13(4):1148–1164

Rathore LS, Mohapatra M, Geetha B (2017) Collaborative mechanism for tropical cyclone monitoring and prediction over North Indian Ocean. In: Tropical Cyclone Activity over the North Indian Ocean, pp 3-27. Springer, Cham. https://doi.org/10.1007/978-3-319-40576-6_1

Reddy BR, Srinivas CV, Venkatraman B (2022) Observational analysis and numerical simulation of sea breeze using WRF model over the Indian southeast coastal region. Meteorol Atmos Phys 134(3):57

Reddy BR, Srinivas CV, Venkatraman B (2023) Impact of sea-breeze circulation on the characteristics of convective thunderstorms over southeast India. Meteorol Atmos Phys 135(1):5

Sangani DJ, Thakker RA, Panchal SD, Gogineni R (2021) Pansharpening of satellite images with convolutional sparse coding and adaptive PCNN-based approach. J Indian Soc Remote Sens 49(12):2989–3004

Schenkel BA, Hart RE (2012) An examination of tropical cyclone position, intensity, and intensity life cycle within atmospheric reanalysis datasets. J Clim 25(10):3453–3475

Scoccimarro Enrico, Fogli Pier Giuseppe, Reed Kevin A, Gualdi Silvio, Masina Simona, Navarra Antonio (2017) Tropical cyclone interaction with the ocean: The role of high-frequency (subdaily) coupled processes. J Clim 30(1):145–162

Singh OP, Ali Khan TM, Rahman MS (2000) Changes in the frequency of tropical cyclones over the north Indian Ocean. Meteorol Atmos Phys 75(1–2):11–20. https://doi.org/10.1007/s007030070011

Skamarock WC, Klemp JB, Dudhia J, Gill DO, Liu Z, Berner J, Wang W, Powers JG, Duda MG, Barker DM, Huang XY (2019) A description of the advanced research WRF model version 4. NCAR tech. note 556(145):1–192

Srinivas CV, Yesubabu V, Prasad DH, Prasad KH, Greeshma MM, Baskaran R, Venkatraman B (2018) Simulation of an extreme heavy rainfall event over Chennai, India using WRF: Sensitivity to grid resolution and boundary layer physics. Atmos Res 210:66–82

Swapna M, Raju R, Nayak RK, Mohanty PC, SeshaSai MVR, Kumar R (2023) Spatiotemporal characteristics of thermal fronts in relation to potential fishing zones in the continental shelf sea around India. J Indian Soc Remote Sens 51(2):335–348

Takakura T, Kawamura R, Kawano T, Ichiyanagi K, Tanoue M, Yoshimura K (2018) An estimation of water origins in the vicinity of a tropical cyclone's center and associated dynamic processes. Clim Dyn 50:555–569

Thompson G, Field PR, Rasmussen RM, Hall WD (2008) Explicit forecasts of winter precipitation using an improved bulk microphysics scheme. Part II: Implementation of a new snow parameterization. Mon Weather Rev 136(12):5095–5115

Tyagi B, Krishna VN, Satyanarayana ANV (2011) Study of thermodynamic indices in forecasting pre-monsoon thunderstorms over Kolkata during STORM pilot phase 2006–2008. Nat Hazards 56(3):681–698

Umakanth N, Satyanarayana GC, Simon B, Rao MC (2020) Satellite based interpretation of stability parameters on convective systems over India and Srilanka. Asian J Atmos Environ 14(2):119–132

Umakanth N, Satyanarayana GC, Naveena N, Srinivas D, Rao DB (2021) Statistical and dynamical based thunderstorm prediction over southeast India. J Earth Syst Sci 130:1–18

Umakanth N, Kalyan SSS, Satyanarayana GC, Gogineni R, Nagarjuna A, Naveen R, Rao KR, Rao MC (2022) Increasing pre-monsoon rain days over four stations of Kerala, India. Acta Geophys 70(2):963–978

Walsh KJE, McBride JL, Klotzbach PJ, Balachandran S, Camargo SJ, Holland G, Sugi MM (2016) Tropical cyclones and climate change. WIREs Clim Change 7:65–89. https://doi.org/10.1002/wcc.371

Wang Z, Montgomery MT, Dunkerton TJ (2010) Genesis of pre-hurricane Felix (2007). Part I: the role of the easterly wave critical layer. J Atmos Sci 67(6):1711–1729

Webster PJ, Holland GJ, Curry JA, Chang HR (2005) Changes in tropical cyclone number, duration, and intensity in a warming environment. Science 309(5742):1844–1846

Wheeler MC, Hendon HH (2004) An all-season real-time multivariate MJO index: Development of an index for monitoring and prediction. Mon Wea Rev 132:1917–1932

Wilks DS (2006) Statistical methods in the atmospheric sciences, 2nd edn. Academic Press, London

Wing AA, Camargo SJ, Sobel AH, Kim D, Moon Y, Murakami H, Reed KA, Vecchi GA, Wehner MF, Zarzycki C, Zhao M (2019) Moist static energy budget analysis of tropical cyclone intensification in high-resolution climate models. J Clim 32(18):6071–6095

Wu L, Su H, Fovell RG, Dunkerton TJ, Wang Z, Kahn BH (2015) Impact of environmental moisture on tropical cyclone intensification. Atmos Chem Phys 15(24):14041–14053